Ecography

ECOG-04836

Eme, D., Anderson, M. J., Myers, E. M. V., Roberts, C. D. and Liggins, L. 2020. Phylogenetic measures reveal eco-evolutionary drivers of biodiversity along a depth gradient. – Ecoraphy doi: 10.1111/ecog.04836

Supplementary material

Supplementary information

Appendix 1: Supplementary methods, results and figures related to the simulation study informing the conceptual framework.

Building a conceptual framework using simulations to infer the influence of varying speciation and extinction rates on several biodiversity measures.

There are several statistical approaches that can estimate speciation and extinction rates directly from phylogenies; however, these approaches may not perform well for phylogenies limited to a community sample or regional species pool. For instance, in our study we have a list of species derived from an ecological sampling program that yields a largely incomplete phylogeny of ray-finned fishes. This may bias inferences obtained using typical phylogenetic tree-based measures of rates of speciation or extinction, despite the fact that some methods can handle a certain proportion of missing taxa (Davis et al. 2013). Furthermore, the statistical approaches that can estimate speciation and extinction rates directly from phylogenies are largely unable to handle multiple locations, or species present in multiple states (Fitzjohn, 2012). For these reasons, we developed a simulation framework, varying both the speciation and extinction rates, to produce different scenarios and thereby assess the performance of five complementary phylogenetic diversity metrics in capturing different aspects of the phylogenetic structure produced under a variety of carefully articulated scenarios.

To build our conceptual framework presented in Figure 1, we modeled the variation of the species richness, Phylogenetic Diversity (PD), Mean Pairwise Distance (MPD), Variance of the Pairwise Distance (VPD), Mean Nearest Taxonomic Distance (MNTD), and Variance of the Nearest Taxonomic Distance (VNTD) while varying the speciation rate and extinction rates of the phylogeny for the underlying communities. We developed four sets of simulations:

First, we reconstructed 100 phylogenetic trees of a "neutral" community based on a constant birth-death process through time during 60-time-steps using a speciation rate of 0.09 per time unit, and an extinction rate of 0.03 per time unit (e.g. per million of years). These rates are comparable to those found in empirical studies of several different taxonomic groups (Jetz et al. 2012; Stadler and Bokma 2013; Matschiner et al. 2017; Rabosky et al. 2013, 2018). Then, we explored the phylogenetic landscape by increasing and decreasing the "neutral" speciation and extinction rates by 10, 20, 30, 40 and 50% for a total of 121 combinations of parameters. For each combination of parameters, 100 trees were constructed, and the mean of the different biodiversity measures estimated. This combination of parameters enabled exploration of the variation in the six biodiversity measures considering the four main scenarios presented in Figure 1.b (i.e. high speciation and low extinction, high speciation and extinction, high extinction and low speciation, low speciation and extinction). In this first set of simulations, all extant species simulated in the community were included in the calculation of the biodiversity indices. However, in practice, most studies sample 'communities' that represent only a fraction of the overall diversity of a regional species pool and/or phylogenetic tree (also called incomplete taxon sampling). Consequently, inference of biodiversity measures based on all species within the phylogeny may differ from those based on a sampled community (Fitzjohn et al. 2009; Hohna et al., 2011; Cusimano et al. 2012; Hohna 2014).

In the second set of simulations, we only considered a random fraction (50% and 20%) of the extant species represented in the phylogeny in the calculation of the six biodiversity measures. This second set of simulations enabled us to assess how subsampling of the complete phylogeny (similar to a 'community' sample) affects the six biodiversity measures and our inference. Here, we also considered trees simulated with 60 time-steps. In these first two sets of simulations, the speciation rate and the extinction rate were constant through time. However, it is well known that the diversification rate (speciation-extinction) can be heterogeneous through time (Stadler 2011; Morlon et al. 2011; Jetz et al. 2012; Morlon 2014; Alfaro et al. 2018; Jetz and Pyron 2018; Henao Diaz et al. 2019). For instance, mass extinction events dramatically increase the extinction rate for a short period of time and can considerably affect the extant communities and their phylogenetic structure (Krug et al. 2009; Alroy, 2010; Harnik et al. 2012; Sanmartín

and Meseguer 2016). Moreover, along a gradient of decreasing environmental/geological stability, the frequency of extinction events and their strength is expected to increase (e.g. Pleistocene glaciation in Northern Europe and Northern America, Hewitt 2004; Jablonski 2008).

The third set of simulations was used to develop the conceptual figure (Figure 1.b), and included variation in the extinction rate as an increase in the frequency and strength of the mass extinction events (also called 'episodic birth-death model' or 'mass extinction model', Sanmartín and Meseguer, 2016). Increasing evidence for mass extinction events across geological time (Harnik et al. 2012; Kocsis et al. 2019) suggest that this variable extinction rate is more likely than a constant extinction rate through time. We simulated 7 scenarios of increasing extinction through time, using an extinction rate of 0.03, and 60 time-steps for all scenarios: 1) Constant extinction rate of 0.03 per time unit through evolutionary history; 2) one extinction event after 10 time-steps with 50% survival probability; 3) one extinction event after 10 time-steps with 20% survival probability; 4) two extinction events after 10 and 25 time-steps with 50% survival probability for both; 5) two extinction events after 10 and 25 time-steps with 20 and 50% survival probabilities; 6) two extinction events after 10 and 25 time-steps with 20% survival probability for both; and 7) three extinction events after, 10, 25 and 35 time-steps with 20, 20 and 50% survival probabilities respectively. For each scenario, we increased and decreased the neutral extinction rate of 0.09 by 10, 20, 30, 40, 50%. The speciation rate was assumed to be constant through time. In total, we modelled 77 combinations of parameters and for each combination 100 trees were simulated, and the 6 biodiversity measures calculated. To mimic an intermediate neutral scenario here, we considered the same speciation rate at 0.09 per time unit and simulated according to scenario 4 (with two mass extinction after 10 and 25 time-steps with 50% survival probability for both).

Finally, the fourth set of simulations was similar to the third set except that only a random fraction (i.e. 50% and 20%) of the extant species were considered to compute the six biodiversity measures.

For each set of simulations and every combination of parameters we computed the average of the six biodiversity measures over the 100 simulated trees, and built a heatmap to display positive or negative deviation of the metric from the expected neutral community (centre of figures A1, A3, A5, A7). The average simulated trees for extreme combinations of parameters were also presented (including the neutral community). To select the average simulated tree for a given combination of parameters, we normalized the values for each biodiversity metric (to give them the same weight), then summed the absolute normalized value for each simulated tree, and selected the tree with the smallest value (smallest distance to the average for all the biodiversity measures). The correlation among different random fractions of species in the second and fourth set of simulations were calculated using the Spearman coefficient.

All simulations were performed in R (R core Team, 2018). We used the *tess.sim.age* function of the TESS R package (Hohna 2013) to simulate the trees, and the ape R package (Paradis and Schliep 2018) to display the trees.

Supplementary figures for the simulations:

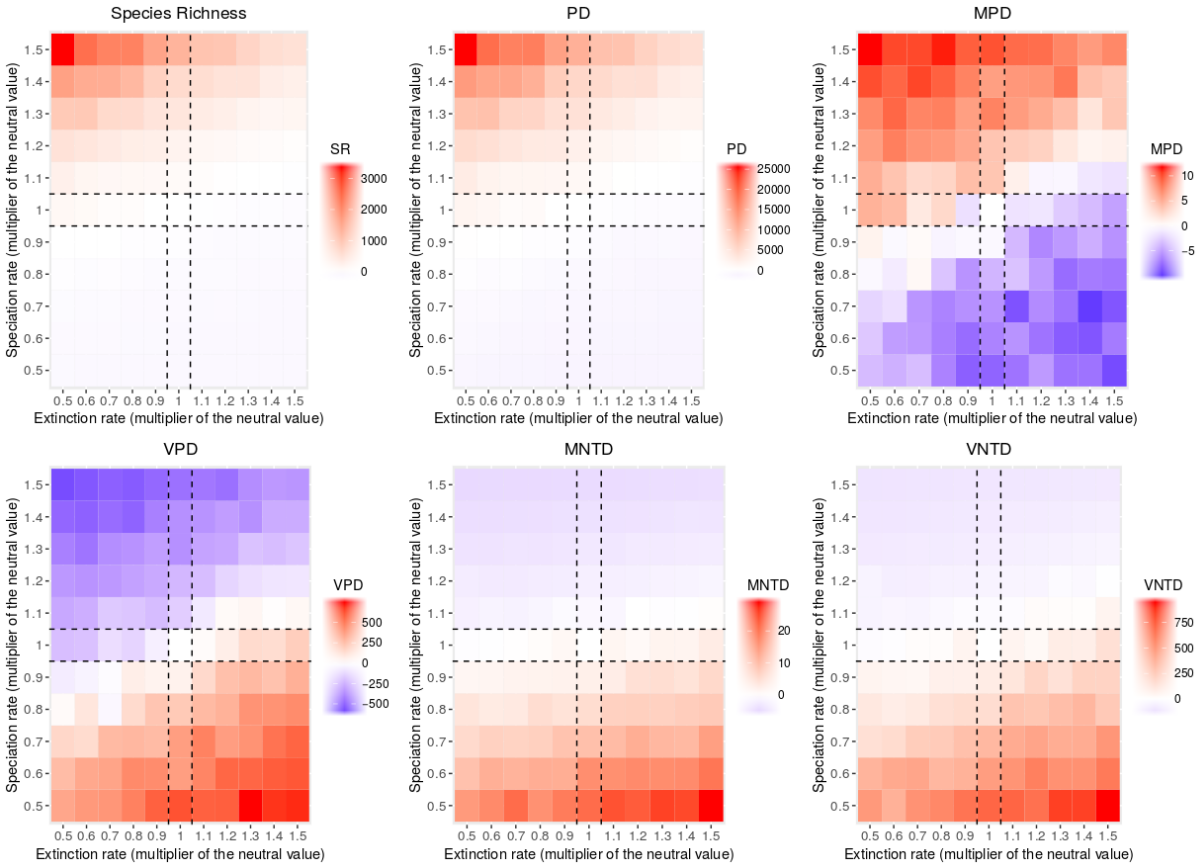

Figure A1: Variation in the species richness (SR), phylogenetic diversity (PD), mean pairwise distance (MPD), variance of the pairwise distance (VPD), mean nearest taxonomic distance (MNTD), and variance of the nearest taxonomic distance (VNTD) across communities with differing speciation and extinction rates using a constant birth-death model (i.e. first set of simulations). Color represents the deviation of the simulated community from the "neutral" community represented in the centre (i.e. in white). The biodiversity measures correspond to the average of 100 simulated trees for each combination of speciation and extinction parameters. Trees were simulated considering 60 time-steps, and the neutral speciation and extinction rates were 0.09 and 0.03 respectively.

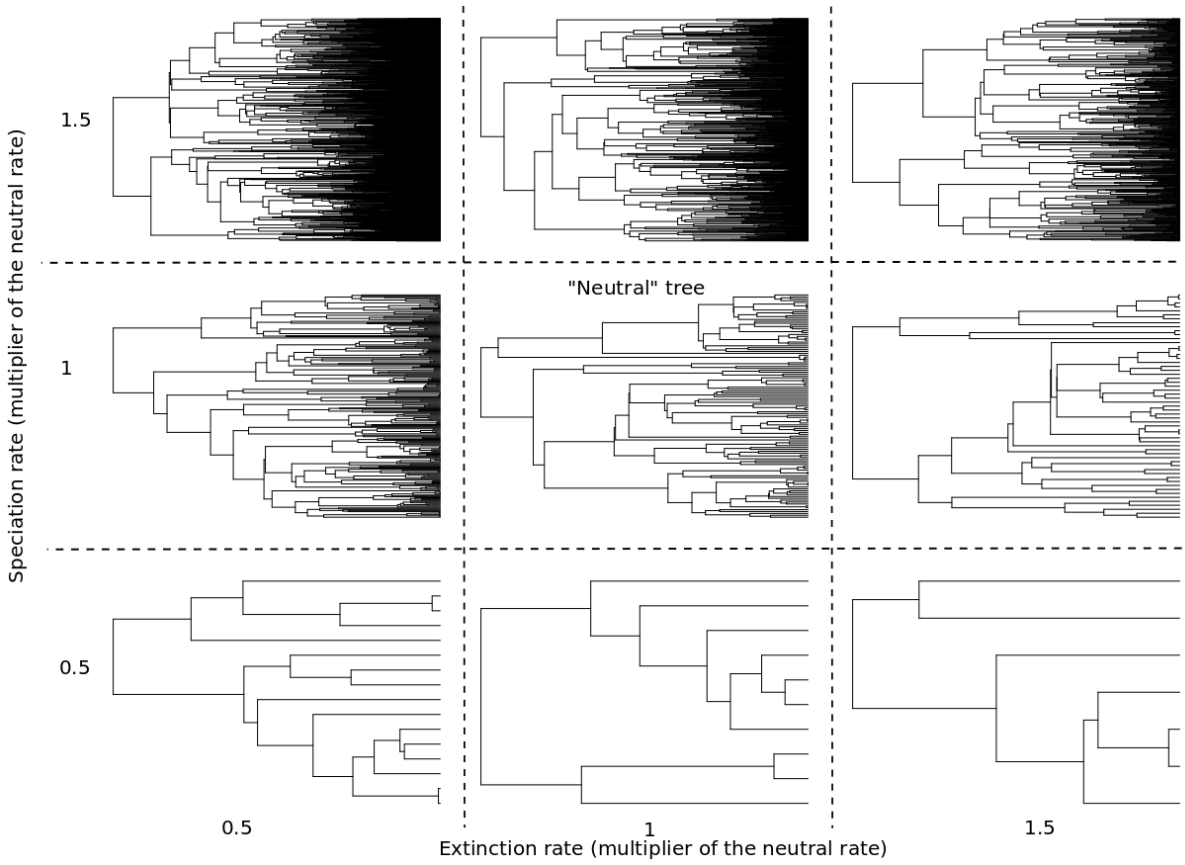

Figure A2: Average simulated trees across a range of speciation and extinction rates using a constant birth-death model. The trees were simulated using 60 time-steps. Only average trees with extreme (0.5 and 1.5 times the neutral rate) and neutral speciation (i.e. 0.09 per time unit) and extinction rates (i.e. 0.03 per time unit) are displayed.

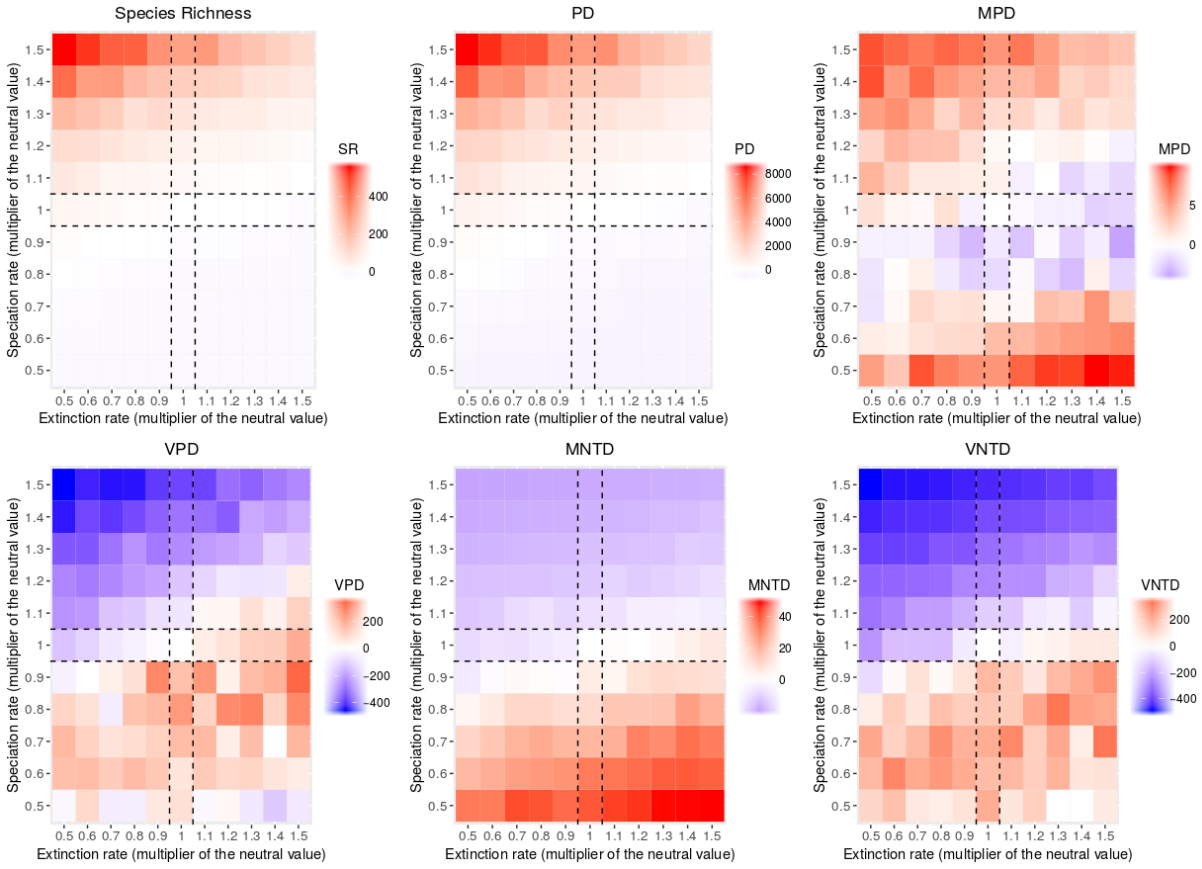

Figure A3: Variation in the species richness (SR), phylogenetic diversity (PD), mean pairwise distance (MPD), variance of the pairwise distance (VPD), mean nearest taxonomic distance (MNTD), and variance of the nearest

taxonomic distance (VNTD) across communities with differing speciation and extinction rates using a constant birth-death model, but randomly subsampling 20% of the extant species (i.e. second set of simulations).

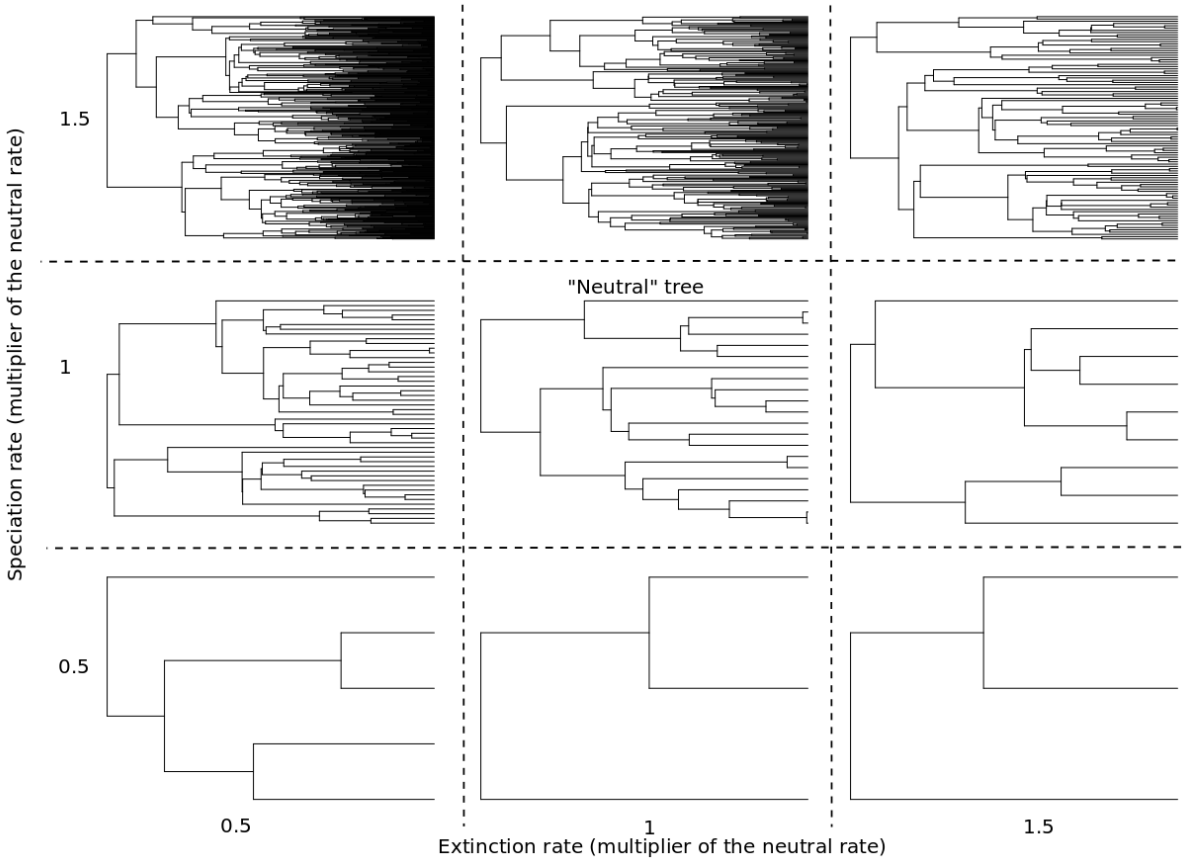

Figure A4: Average simulated trees across a range of speciation and extinction rates using a constant birth death model, but subsampling randomly 20% of the extant species. The trees were simulated using 60 time-steps. Only average trees with extreme (0.5 and 1.5 times the neutral rate) and neutral speciation (i.e. 0.09 per time unit) and extinction rates (i.e. 0.03 per time unit) are displayed.

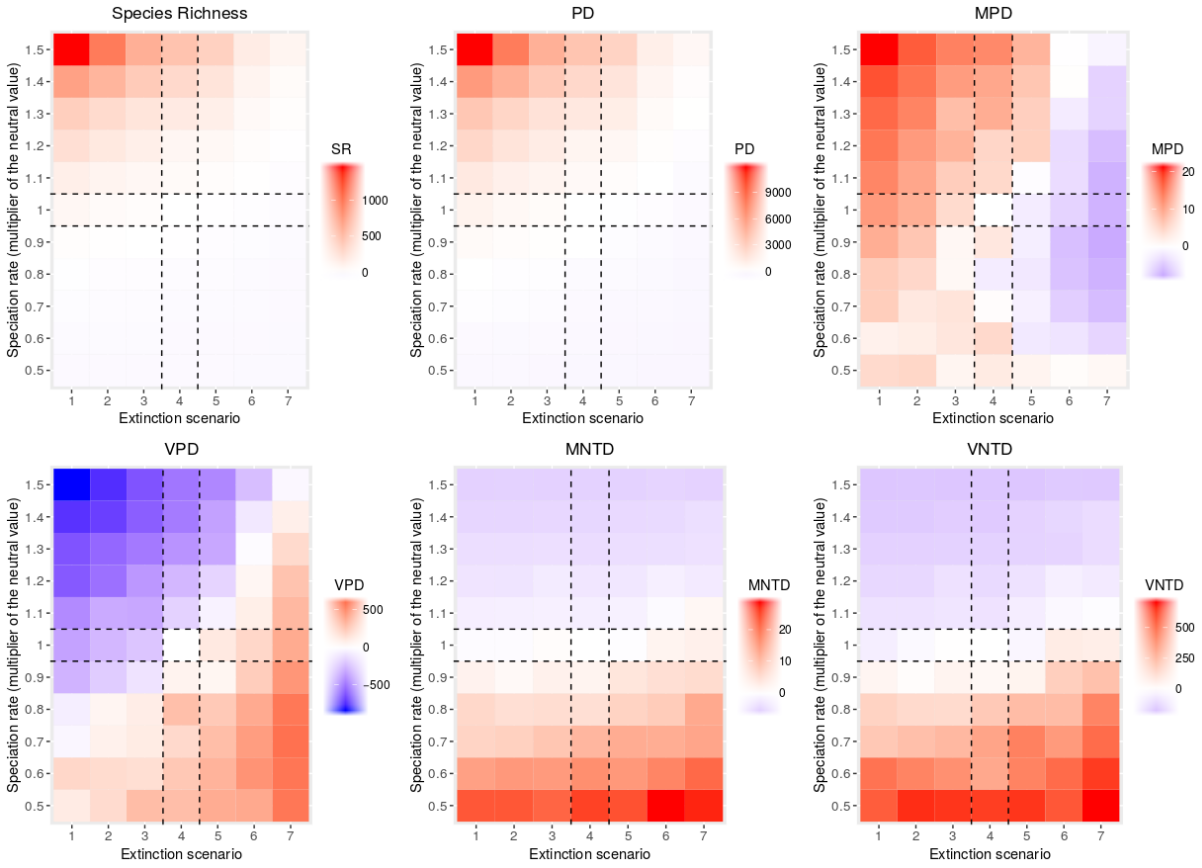

Figure A5: Variation in the species richness (SR), phylogenetic diversity (PD), mean pairwise distance (MPD), variance of the pairwise distance (VPD), mean nearest taxonomic distance (MNTD), and variance of the nearest taxonomic distance (VNTD) across communities with differing speciation rates and differing frequency and strength of mass extinction events (i.e. extinction scenario, third set of simulations) using a constant birth death model. Increasing the frequency and the strength of mass extinction events emulated a periodic mass extinction events caused by high environmental and/or geologic instability (variability) through evolutionary history. This third scenario was used to develop the conceptual figure (Figure 1.b). Extinction scenario: 1) Constant extinction rate of 0.03 per time unit through evolutionary history; 2) one extinction event after 10 time-steps with 50% survival probability; 3) one extinction event after 10 time-steps with 20% survival probability; 4) two extinction events after 10 and 25 time-steps with 50% survival probability for both; 5) two extinction events after 10 and 25 time-steps with 20 and 50% survival probabilities; 6) two extinction events after 10 and 25 time-steps with 20% survival probability for both; and 7) three extinction events after, 10, 25 and 35 time-steps with 20, 20 and 50% survival probabilities respectively.

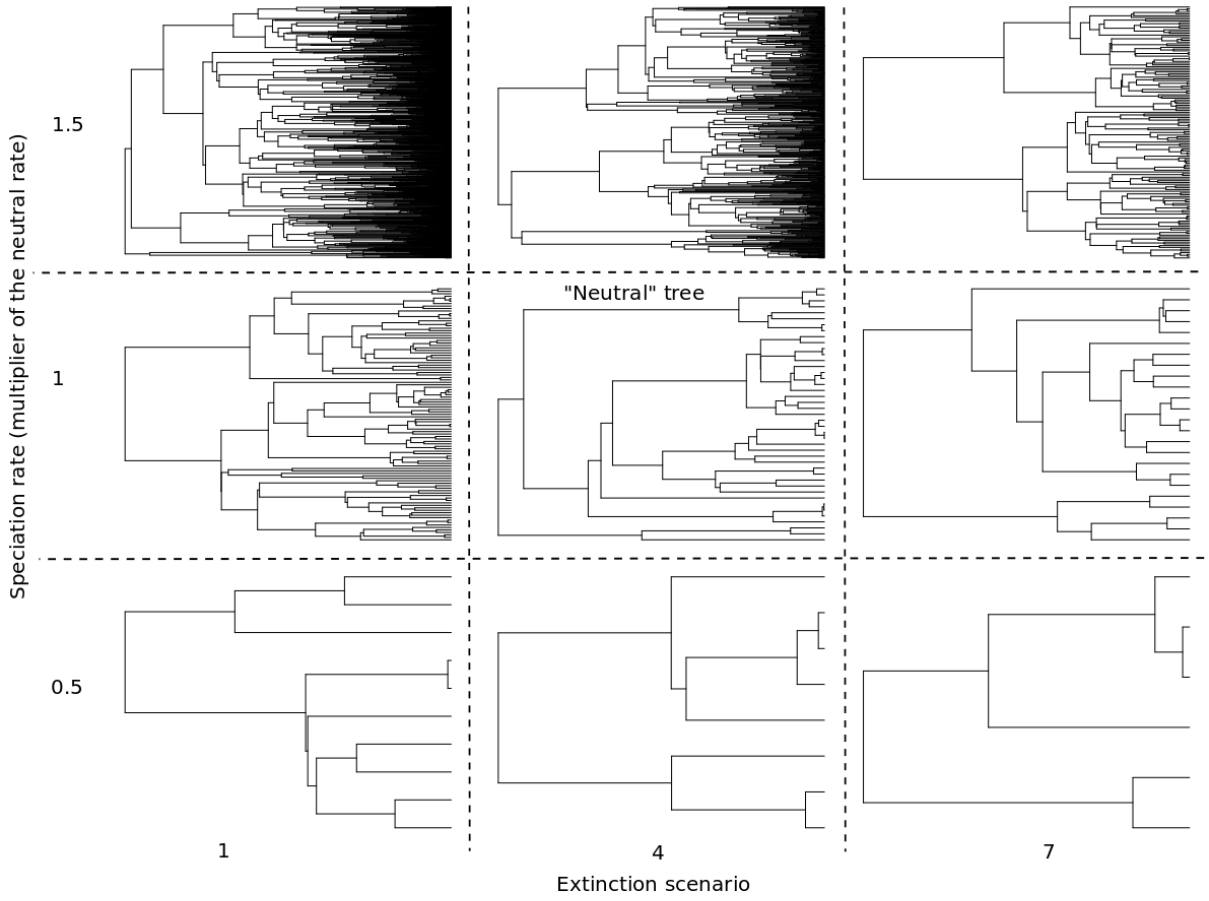

Figure A6: Average simulated trees across a range of speciation rates and varying frequency and strength of mass extinction events (i.e. extinction scenario) using a constant birth-death model. The trees were simulated using 60 time-steps. Only average trees with the two extreme speciation rates (0.5 and 1.5 times the neutral rate of 0.09 per time unit) and the two extreme extinction scenarios (1 and 7) are displayed in addition to the average "neutral" tree (i.e. speciation rate of 1*0.09, and extinction scenario 4). Extinction scenario: 1) Constant extinction rate of 0.03 per time unit throughout the evolutionary history; 4) two extinction events after 10 and 25 time-steps with 50% survival probability for both; and 7) three extinction events after, 10, 25 and 35 time-steps with 20, 20 and 50% survival probabilities respectively.

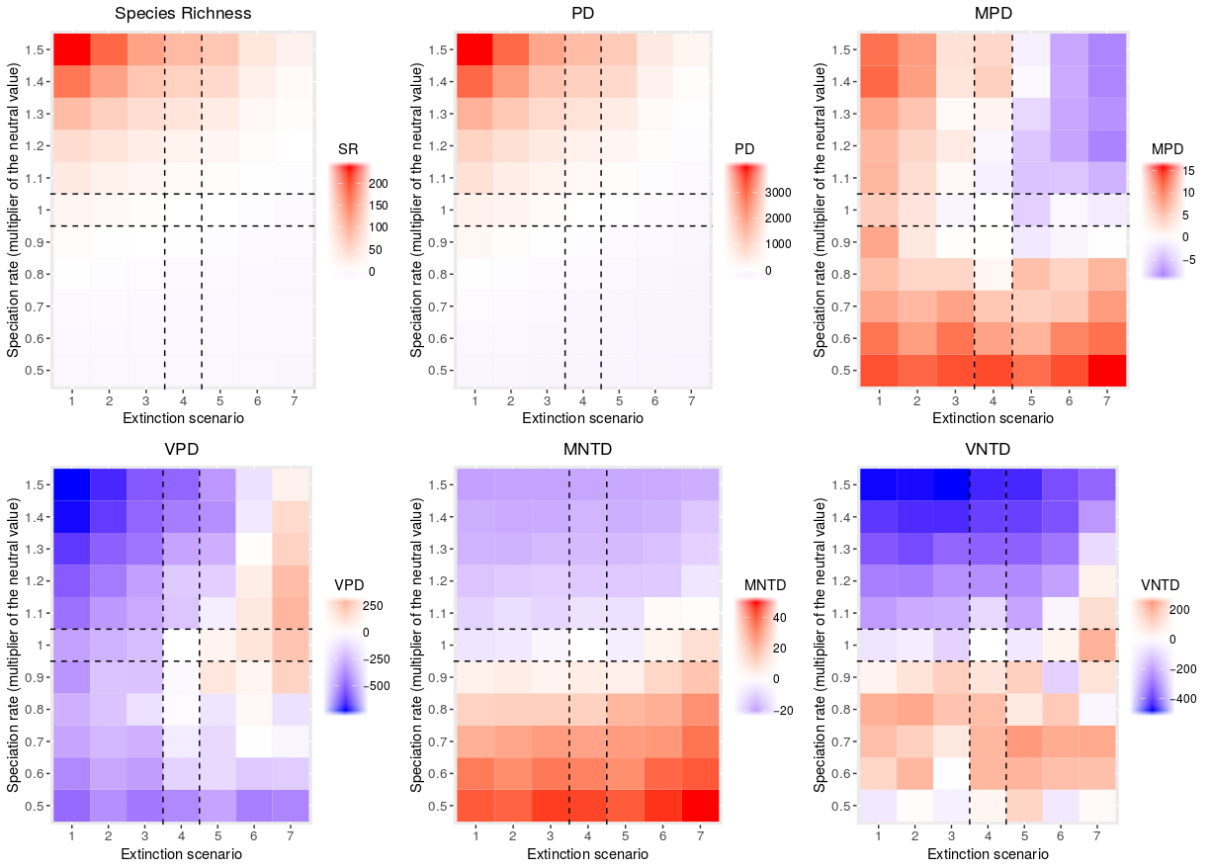

Figure A7: Variation in the species richness (SR), phylogenetic diversity (PD), mean pairwise distance (MPD), variance of the pairwise distance (VPD), mean nearest taxonomic distance (MNTD), and variance of the nearest taxonomic distance (VNTD) across communities with different speciation rates and differing frequency and strength of mass extinction events (i.e. extinction scenario) using a constant birth death model, but randomly subsampling 20% of the extant species (i.e. fourth set of simulations). Extinction scenario: 1) Constant extinction rate of 0.03 per time unit through evolutionary history; 2) one extinction event after 10 time-steps with 50% survival probability; 3) one extinction event after 10 time-steps with 20% survival probability; 4) two extinction events after 10 and 25 time-steps with 50% survival probability for both; 5) two extinction events after 10 and 25 time-steps with 20 and 50% survival probabilities; 6) two extinction events after 10 and 25 time-steps with 20% survival probability for both; and 7) three extinction events after, 10, 25 and 35 time-steps with 20, 20 and 50% survival probabilities respectively.

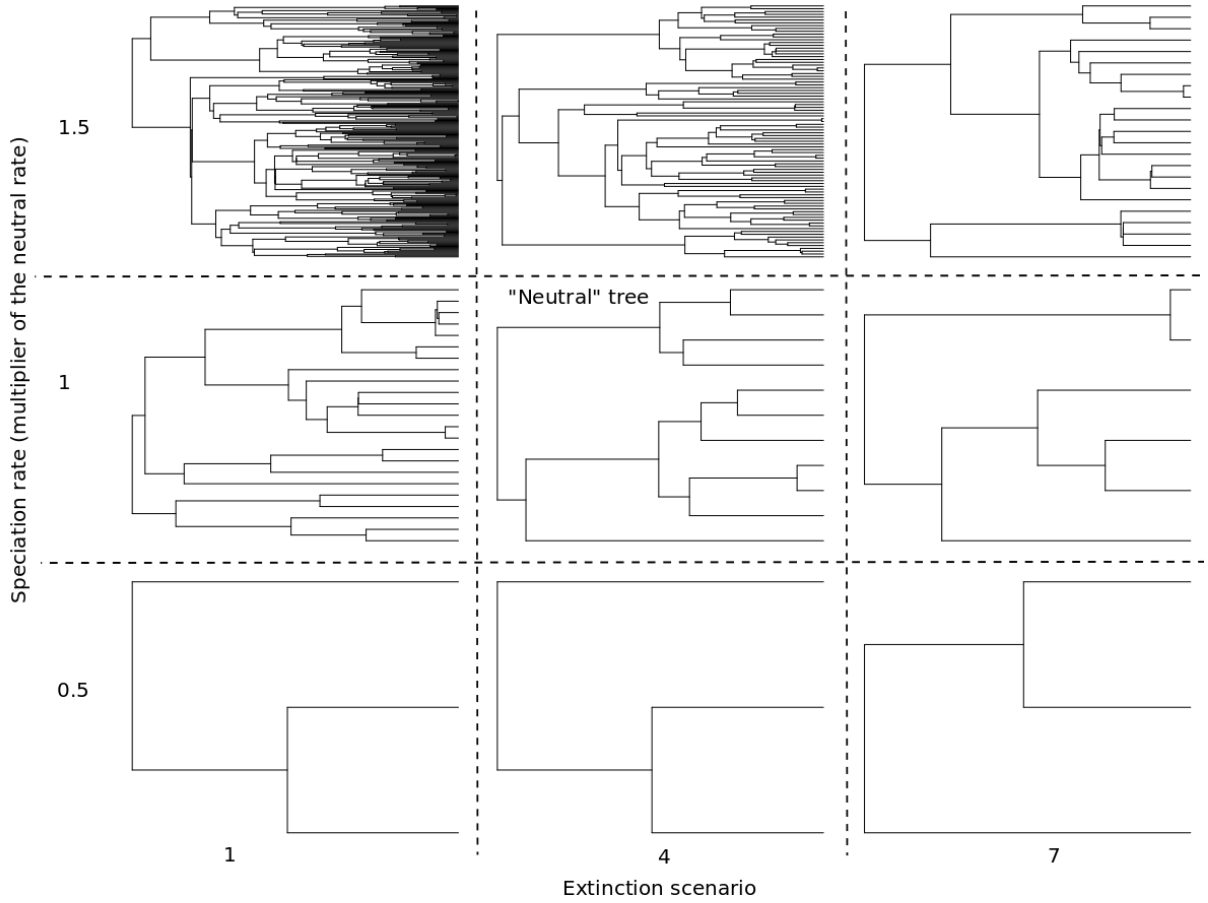

Figure A8: Average simulated trees across a range of speciation rates and varying frequency and strength of mass extinction events using a constant birth-death model, but randomly subsampling 20% of the extant species. The trees were simulated including 60 time-steps. Only average trees with the two extreme speciation rates (0.5 and 1.5 times the neutral rate of 0.09 per time unit) and the two extreme extinction scenarios (1 and 7) are displayed in addition to the average "neutral" tree (i.e. speciation rate of 1*0.09, and extinction scenario 4). Extinction scenario: 1) Constant extinction rate of 0.03 per time unit through evolutionary history; 4) two extinction events after 10 and 25 time-steps with 50% survival probability for both; 7) three extinction events after, 10, 25 and 35 time-steps with 20, 20 and 50% survival probabilities respectively.

Table A1: Spearman coefficient of correlation among metrics using different sampling fraction (1 = 100%, 0.5 =50%, 0.2 = 20%), for the simulations with, and without, mass extinction events.

Mass.Extinction	fraction1	fraction2	SR	PD	MPD	VPD	MNTD	VNTD
No	1	0.5	0.998	0.998	0.881	0.982	0.997	0.992
No	0.5	0.2	0.998	0.998	0.500	0.844	0.995	0.901
No	1	0.2	0.998	0.997	0.238	0.814	0.994	0.893
Yes	1	0.5	0.998	0.998	0.861	0.945	0.991	0.985
Yes	0.5	0.2	0.997	0.998	0.650	0.755	0.992	0.842
Yes	1	0.2	0.998	0.997	0.312	0.594	0.992	0.830

Simulation results:

Within each set of simulations, clear differences in the variation of the metrics across the speciation and extinction landscape can be seen. For most of the metrics except MPD and VPD, these variations remain relatively robust to the

change of extinction through time and the inclusion of mass extinction events (i.e. “episodic birth death model” presented in set 3 and 4) and the random sub-sampling of a fraction of the extant species (set 2 and 4). For all sets of simulations species richness and PD were sensitive to the variation of speciation and extinction and were maximal with high speciation and low extinction (see top left corner in Figure A1, A3, A5, A7). MNTD and VNTD were mostly sensitive to the change in the speciation rate regardless of the set of simulations used and were minimal with high rates of speciation (Figure A1, A3, A5, A7). On the contrary, MPD and VPD were affected by variation of both speciation and extinction, and even more so when mass extinction events were strong, frequent, and recent (Figure A1, A4). This removal of lineages early in the phylogenetic history decreased the average length among species and even more so if strong extinction events appear late in the evolutionary history (i.e. close to present), leading to low MPD values (Figure S6). This same process also positively affects the variance of the distance among species (VPD). Indeed, phylogenies affected by strong and frequent mass extinction showed long basal branches and young crown groups (also called “a “broom-and-handle” shape, Sanmartín and Meseguer 2016; Figure S5, S6). The signature of the strong variation of extinction through time (including mass extinction events) can be erased quickly if the speciation rate increases quickly afterward (i.e. the “rebound effect”, Alroy 2008) or if the strength and the time of the extinction is clade dependent (Rabosky 2010; Stadler 2011). Nonetheless, our simulations evidence that with simple scenarios and using the panel of biodiversity measures we are able to capture the signature of extinction events in the phylogenetic structure.

The random sampling of a fraction of the extant species, mostly affected the variation of the MPD, and to a lesser extent VPD and VNTD across the speciation and extinction landscape for both sets of simulations including the constant birth-death model and the episodic birth-death model (i.e. including mass extinction events, Table A1). Indeed, for MPD, the Spearman coefficient of correlation decreased sharply when comparing communities including 100%, 50% and 20% of the extant species (Table A1). The greatest discrepancies appeared when the speciation rate was extremely low (bottom rows in Figure A1, A3 and Figure A5, A7). The combination of low speciation rates, the random selection of a small fraction of the extant species, and early divergence of the phylogenetic tree imposed by the *tess.sim.age* function may have overly constrained the shape of the phylogenies that included only a handful of species with long branches, increasing MPD and VPD (Figure A4, A8). For other biodiversity measures, the sub-sampling of a random fraction did not qualitatively affect the variation of the metrics throughout the landscape of varying speciation and extinction parameters (Table A1, Figure A1, A3, A5, A7). Additional testing would be required to further understand the impact of non-random sampling strategies, as it has been recognized that sampling strategy can affect the shape of the phylogeny and the inferences about the underlying mechanisms (Hohna et al. 2011; Cusimano et al. 2012; Sanmartín and Meseguer 2016).

Appendix 2: Supplementary methods, results and figures related to the empirical study.

Generation of new DNA sequence information for taxa not represented in genetic sequence repositories:

For New Zealand fish taxa within our community matrix, but without existing DNA information, we targeted the mitochondrial Cytochrome Oxidase 1 (*CO1*) and nuclear *RAG1* gene regions. Fishes were collected on several research expeditions undertaken by the Museum of New Zealand Te Papa Tongarewa, Auckland War Memorial Museum Tāmaki Paenga Hira, and Massey University Auckland, over recent years. Tissue samples (white muscle or fin clips) were preserved in 80-98% ethanol and subsequently stored at -80°C, -20°C or 5°C. All DNA extraction, PCR, and sequencing preparation for the focal taxa was carried out at Massey University Auckland. Genomic DNA was extracted using DNeasy Blood and Tissue kits (Qiagen, Valencia, CA), and additionally the Chelex 100 chelating resin extraction protocol (described in Walsh et al. 1991) if the first extraction had low DNA yield. To amplify a portion of the *CO1* gene region, we used either the primers FishF2 and FishR2 (described in Ward et al. 2005), or the primer combination named Fish CO1-2 Cocktail (as described in Ivanova et al. 2007); to amplify RAG1 we used the RAG1 Cocktail (as described in Lopez et al. 2004). All PCRs were conducted using either the MyTaq™ or MyFi™ DNA polymerase kits (Bioline, Australia Pty Ltd, Alexandria, NSW), as per the kit instructions. For the FishF2/FishR2 primer combination, PCR was performed with an initial denaturation at 95°C for 2 mins, followed by 35 cycles (95°C for 45 secs, 54°C for 45 secs, 72°C for 1 min), then a final extension at 72°C for 5 mins. For the Fish CO1-2 primer cocktail, PCR was performed with a denaturation at 94°C for 1 min, followed by an initial 5 cycles (94°C for 30 secs, 50°C for 40 secs, 72°C for 1 min), followed by 35 cycles (94°C for 30 secs, 54°C for 40 secs, 72°C for 1 min), then a final extension at 72°C for 10 mins (as described in Ivanova et al. 2007). PCR for *RAG1* was performed with an initial denaturation at 95°C for 1 min, followed by 45 touchdown cycles (95°C for 30 secs, 54°C - 50°C for 40 secs, 72°C for 1 min), then a final extension at 72°C for 10 mins. PCR amplicons were purified using Applied Biosystems™ ExoSAP-IT™ PCR Product Cleanup Reagents and protocol (Thermo Fisher Scientific, West Palm Beach, FL) and sequenced in both directions by Macrogen Korea.

Tree Building

We followed the procedure of Eme et al. (2019) using the R package *regPhylo* to build phylogenetic trees for the New Zealand marine ray finned fishes (Actinopterygii). We used a 15 gene supermatrix (as in Eme et al. 2019) for 777 teleost species present in New Zealand waters (Roberts et al. 2017), plus 6 outgroup species recognized as sister taxa of Teleostei (Near et al. 2012, Betancur et al. 2013, 2015, 2017; Hughes et al. 2018). New sequences were obtained for the mitochondrial *CO1* and nuclear *RAG1* gene regions to complement the supermatrix, including for 14 species present in our community dataset, but not previously sequenced (see paragraph above for details regarding DNA extraction, PCR, and sequencing). The new *CO1* and *RAG1* sequences were manually aligned to the best alignment retained in Eme et al. (2019). Poorly aligned positions were removed using the less stringent option in Gblocks v.0.91b (Castresana 2000) for *RAG1* while we used the less stringent selection (removing gappy position) in TRIMAL v.1.2rev59 (Capella-Gutíerrez et al. 2009) for the *CO1*. For all other gene regions (*16S, 12S, Cytb, myh6, zic1, plagl2, rhodopsin, mll4, glyt, tbr1, sh3px3, irbp2, enc1*) we used the best alignment retained by Eme et al. (2019). Six other taxa within our community dataset that did not have DNA sequence information, were added into the Bayesian tree reconstruction using conservative topological constraints based on their taxonomic status (see Eme et al. [2020] folder "TopoConstraints", file "Constraints_6sp_NoDNA.csv") , see Eme et al. (2019) for full explanation of method to include taxa without DNA. The final 15 genes supermatrix incorporated 11,860 bp and included 803 species (including 6 outgroup species that do not belong to New Zealand species list), 797 of which had DNA (791 species that had DNA and belong to New Zealand species list), comprising 3,679 DNA sequences total (See Eme et al. [2020], for the table with accession numbers including new sequences submitted to GenBank). From the supermatrix, we determined the best number of partitions and the appropriate substitution model for each partition with PARTITIONFINDER2 v.2.1.1 (Lanfear et al. 2017). We used the BIC criterion to avoid over-parametrization and restricted our search to the substitution models implemented in RAxML (Stamatakis 2014). To avoid spurious phylogenetic relationships due to data deficiency (incomplete taxon/gene sampling) we identified 165 soft topological constraints defining monophyletic groups based on previous phylogenetic works (Near et al. 2012, 2013, Betancur et al. 2013a,b, 2015; Sanciangco et al. 2016) and synthesized in the recent update of the classification of fishes by Betancur et al. (2017) (See Eme et al. [2020] folder "TopoConstraints" file "Const165_DeepfinV4_Table_Topublish.txt" for a list of constraint and DeepFinV4 available at:

https://bmcevolbiol.biomedcentral.com/articles/10.1186/s12862-017-0958-3). The soft constraints were used to build a multifurcating guiding tree to constrain the tree reconstruction by maximum likelihood in RAxML. This step allowed unconstrained taxa to be positioned in the tree based on their molecular affinities while the constrained taxa follow the topology imposed by the guiding tree. Then, we used the bootstrap support to identify nodes with maximal support (100%), which are either nodes with a soft topological constraint or strongly supported by molecular data, in order to define hard topological constraints for the Bayesian reconstruction software BEASTV2.4.7 (Bouckaert et al. 2014). We performed this two-step approach for defining constraints, because BEAST only accommodates hard constraints (i.e. does not allow unconstrained taxa to enter clades) and does not accommodate soft constraints (i.e. to allow unconstrained taxa to enter into 'soft' constrained clades according to their molecular affinities). To place our phylogeny into an absolute time frame, we performed an uncorrelated relaxed clock model (Drummond et al. 2006) in conjunction with the CladeAge (Matschiner et al. 2017) approach implemented in BEAST V2.4.7. Clade Age uses the oldest fossil record of well-defined morphological clades, and estimates of the net diversification rate, diversification turnover, and fossil sampling rate to derive objective prior distributions for calibration points. Here, we followed Eme et al. (2019) and used the first occurrence in the fossil record of 44 well-defined morphological clades (Eme et al. [2020] folder "TopoConstraints" file "Table_44Fossil_CalibrationPoints.txt"), the estimates of the diversification rate and turnover provided by Santini et al. (2009), and the species sampling rate (0.0066-0.01806 $L^{-1}.myr^{-1}$) estimated by Matschiner et al. (2017). For computational feasibility, the super-matrix was partitioned into 7 partitions (one partition for the non-coding mitochondrial, and 2 times 3 partitions for each codon position for the coding mitochondrial and coding nuclear genes, respectively). The tree topology and branch-lengths were linked among partitions, but parameters of the substitution and clock models were free to vary. For each partition, we assumed a GTR+G4 substitution model, with 4 categories of evolutionary rates among sites from a gamma distribution. A birth-death model was used as the speciation model which also allowed positioning of the 6 taxa without DNA information (Khun et al. 2011) according to the hard constraints previously defined. We ran 4 independent Monte Carlo Markov Chains (MCMCs) in BEAST V.2.4.7, with 400 000 000 generations and sampled every 40 000 generations. The runs were individually checked for convergence in TRACER v1.6 (Rambaut et al. 2013) and we removed the first 25% of iterations from each chain as burn-in, before combining them with LOGCOMBINER. We sub-sampled 10,004 trees from the combined posterior distribution with LOGCOMBINER to extract the maximum clade credibility tree (MCCT) with TREEANNOTATOR. The MCCT is displayed in Supplementary Information Figure A9. We randomly extracted 100 trees from the combined posterior distribution of trees and pruned to the 149 species present in the community dataset, to assess the effect of the phylogenetic uncertainty on the phylogenetic diversity metrics (Available in Eme et al. [2020]).

Testing the correlation among phylogenetic diversity metrics

We used the Spearman correlation coefficient to assess the correlation among the phylogenetic diversity metrics calculated for the dataset (n=295 BRUVs communities with at least 2 species) considering the average values of each metric computed over the 100 trees. We used pairwise plots, a nonmetric-Multidimensional scaling (using MASS R package, Venables and Ripley 2002), and a clustering approach (i.e. UPGMA) in R (R core Team 2018) to display relationships among metrics.

Linear mixed model to quantify the variation of the phylogenetic uncertainty in the modeling of the different phylogenetic diversity patterns across depth and latitude.

In order to estimate the proportion of variation explained by the phylogenetic uncertainty in the modeling of the different phylogenetic diversity patterns, we also used a linear mixed effects model including the trees (i.e. TreeID) as a random effect and considering depth and latitude as continuous variables and fixed effects. Quadratic effects and interactions were also considered in the model as fixed effects. We considered as the most complex random structure a random intercept and slope model for both the depth and latitude variables for each tree. To avoid numerical instability the response variables and explanatory variables were normalized before model fitting. Selections of the best random effects were done by fitting the models under restricted maximum-likelihood optimization (REML). The

best structure was determined based on AICc criteria and then we performed the selection of the fixed effects using maximum likelihood (ML) optimization (Zuur et al. 2009). To quantify the variation attributed to the phylogenetic uncertainty (the random factor) in the overall model, we estimated the conditional (including fixed and random effects) and marginal (including fixed effects only) R^2 proposed by Nakagawa and Shielzeth (2013) and generalized to the random intercept and slope model by Johnson (2014). Conditional and marginal effects were computed on the best fixed effects models but fitted under REML optimization (Nakagawa and Shielzeth 2013). We also estimated the relative contribution of each parameter in the model based on semipartial R^2 estimated by the Nakagawa, Shielzeth and Jonhson approach as well as the approach developed by Jaeger et al. (2016) which considers the correlation among observations. The linear mixed effects models were performed with the lme4 (Bates et al. 2015) and nlme R packages (Pinheiro et al. 2016), the AICc and the Nakagawa R^2 were performed using the MuMIn (Bartoń 2016) R package, and semi.partial R^2 were performed using the r2glmm (Jaeger et al. 2017) R package.

Supplementary results

Correlation among metrics

The pairwise correlations among metrics based on our empirical dataset confirmed: 1) the strong correlation between PD and species richness; 2) the absence of a relationship between MPD and species richness; 3) the moderate correlation between VPD and species richness or MPD; 4) the distinction between MPD and MNTD (supported by a moderate relationship); and 5) the independence of MNTD and VNTD (Figure A10). Our empirical dataset supported the classification of the different phylogenetic diversity metrics into the three groups: richness (represented by PD), divergence (represented by MPD and MNTD), and regularity (VPD and VNTD) (Figure A11A, B).

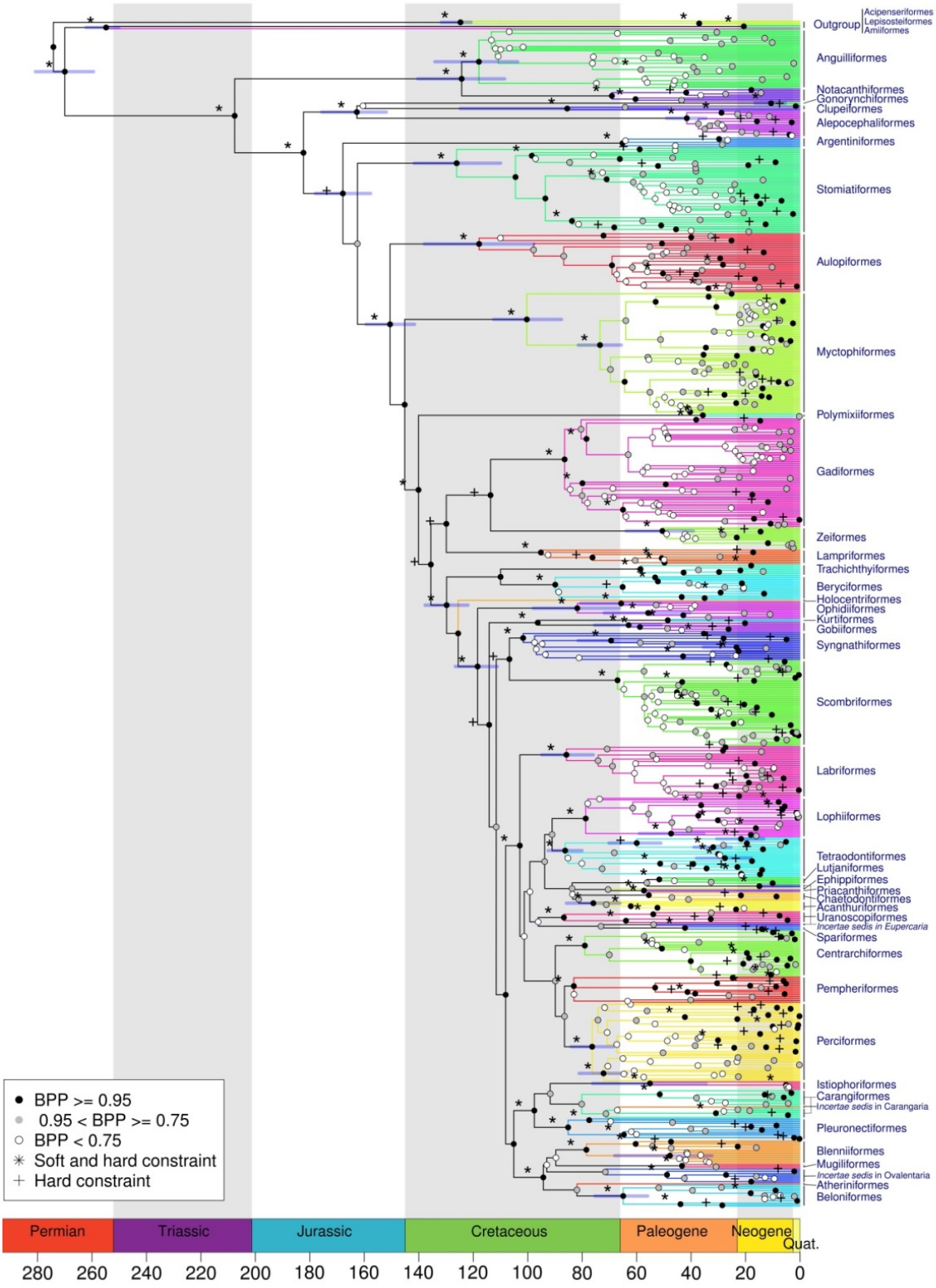

Figure A9: The maximum clade credibility tree (MCCT) of the New Zealand marine ray-finned fishes (including 803 species and composed of 797 in-group species, 791 of which had DNA information, plus 6 outgroup species) based on 15 genes and 44 calibration points. The MCCT is scaled to the geological time-scale with absolute time given in millions of years. Light blue horizontal bars shown at individual nodes extend to the 0.025 and 0.975 quantiles of the posterior distribution of divergence time estimates for the 44 clades used for the calibration (only 40 are displayed on the figure because 4 clades are represented by a single taxon). Different colours correspond to different orders of fishes (class Actinopterygii). Soft topological constraints have been used to guide the RAxML tree, and hard constraints have been used to further constrain the Bayesian phylogeny given the strong bootstrap support provided by the RAxML tree. BPP = Bayesian posterior probability. Examination of the MCCT indicated that the topology and date estimates were agreement with the tree previously published by Eme et al. (2019), and recent large-

scale molecular phylogenies for Actinopterygii (Near et al. 2012, Betancur et al. 2013a, 2017; Alfaro et al. 2018; Hughes et al. 2018).

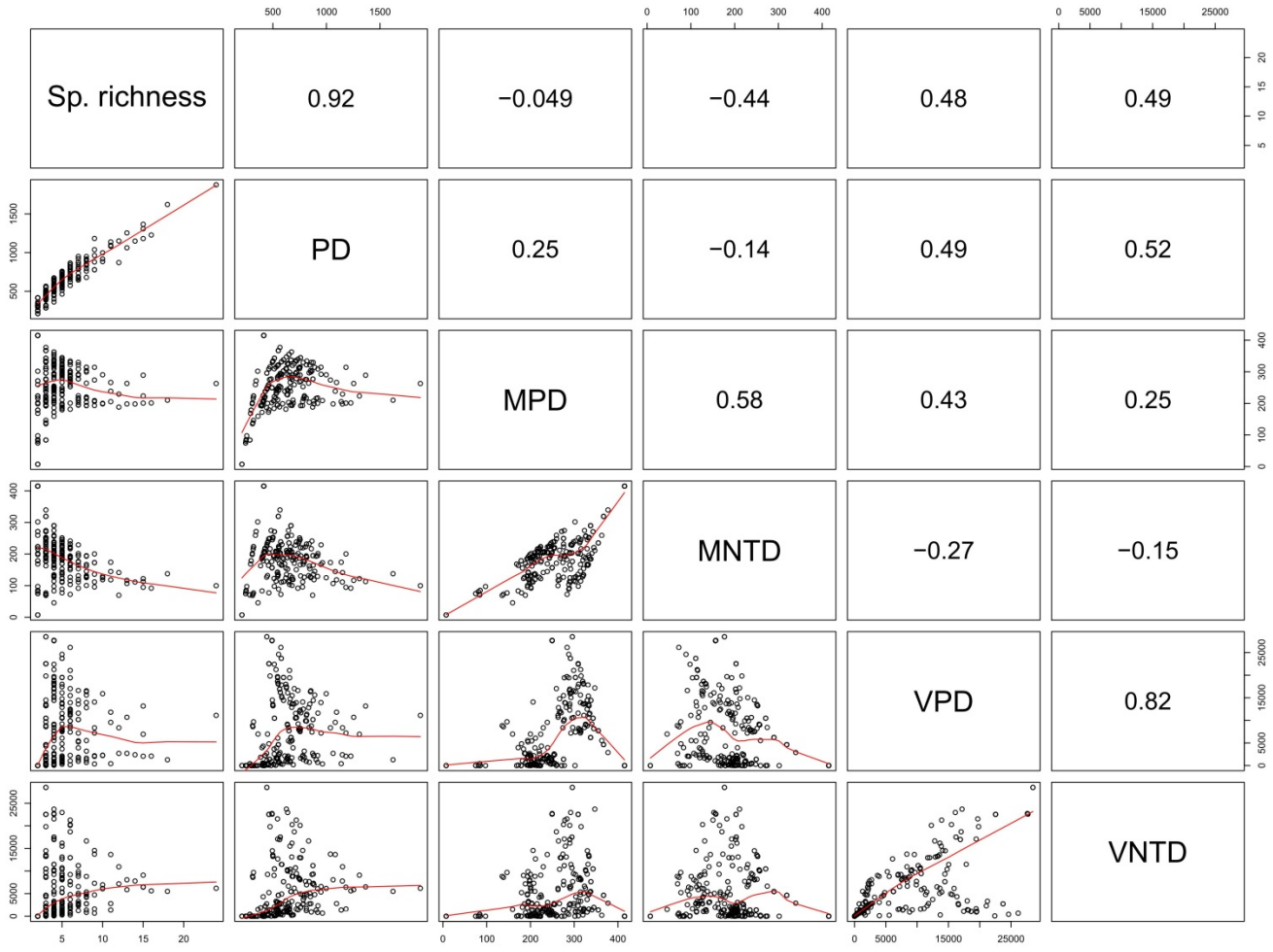

Figure A10: Pairwise relationships among the five phylogenetic diversity measures plus the species richness, based on 295 BRUVs with at least 2 species using the average value obtained from the distribution of 100 trees. The lower panel shows the plot of the data and the red curve represents the fit of a LOEWSS model. The upper panel represents the Spearman correlation coefficient. PD= phylogenetic diversity, MPD= mean pairwise distance, MNTD= mean nearest taxonomic distance, VPD= variance of the pairwise distance, VNTD= variance of the nearest taxonomic distance.

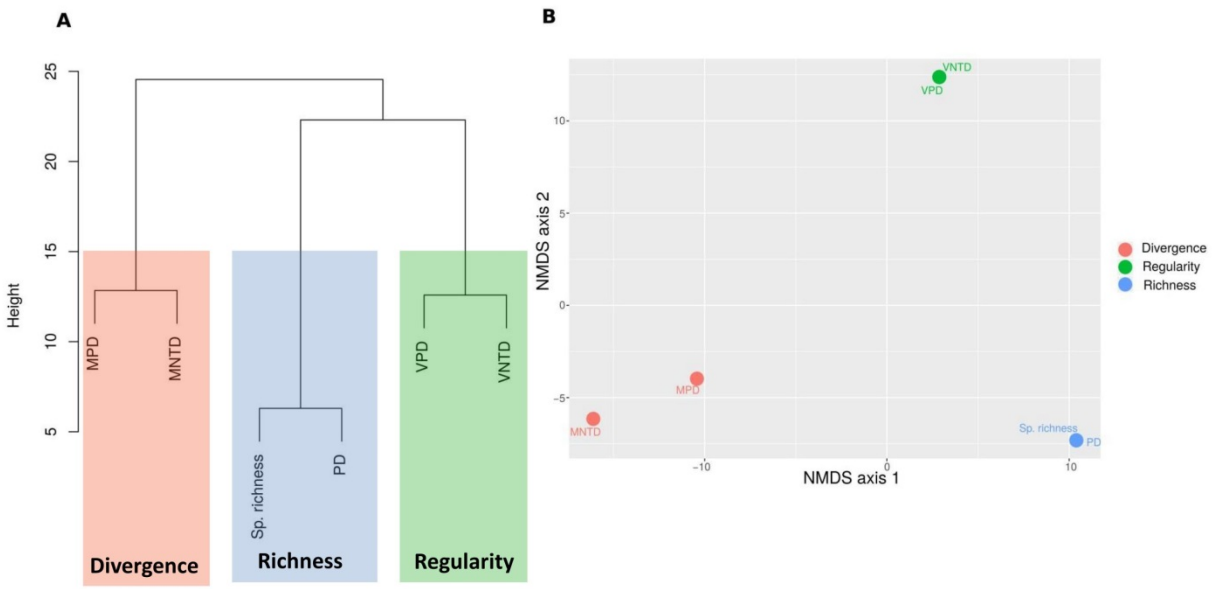

Figure A11: Relationships among metrics and their categories (richness, divergence, regularity) based on the Euclidian distance in multivariate space considering species richness (SR), phylogenetic diversity (PD), mean pairwise distance (MPD), variance of the pairwise distance (VPD), mean nearest taxonomic distance (MNTD), and variance of the nearest taxonomic distance (VNTD) using a A) a clustering approach (UPGMA), and B) a non-metric multidimensional scaling (nMDS) plot showing the first two axis. We used a dataset of 295 BRUVs with at least 2 species using the average value obtained from the distribution of 100 trees.

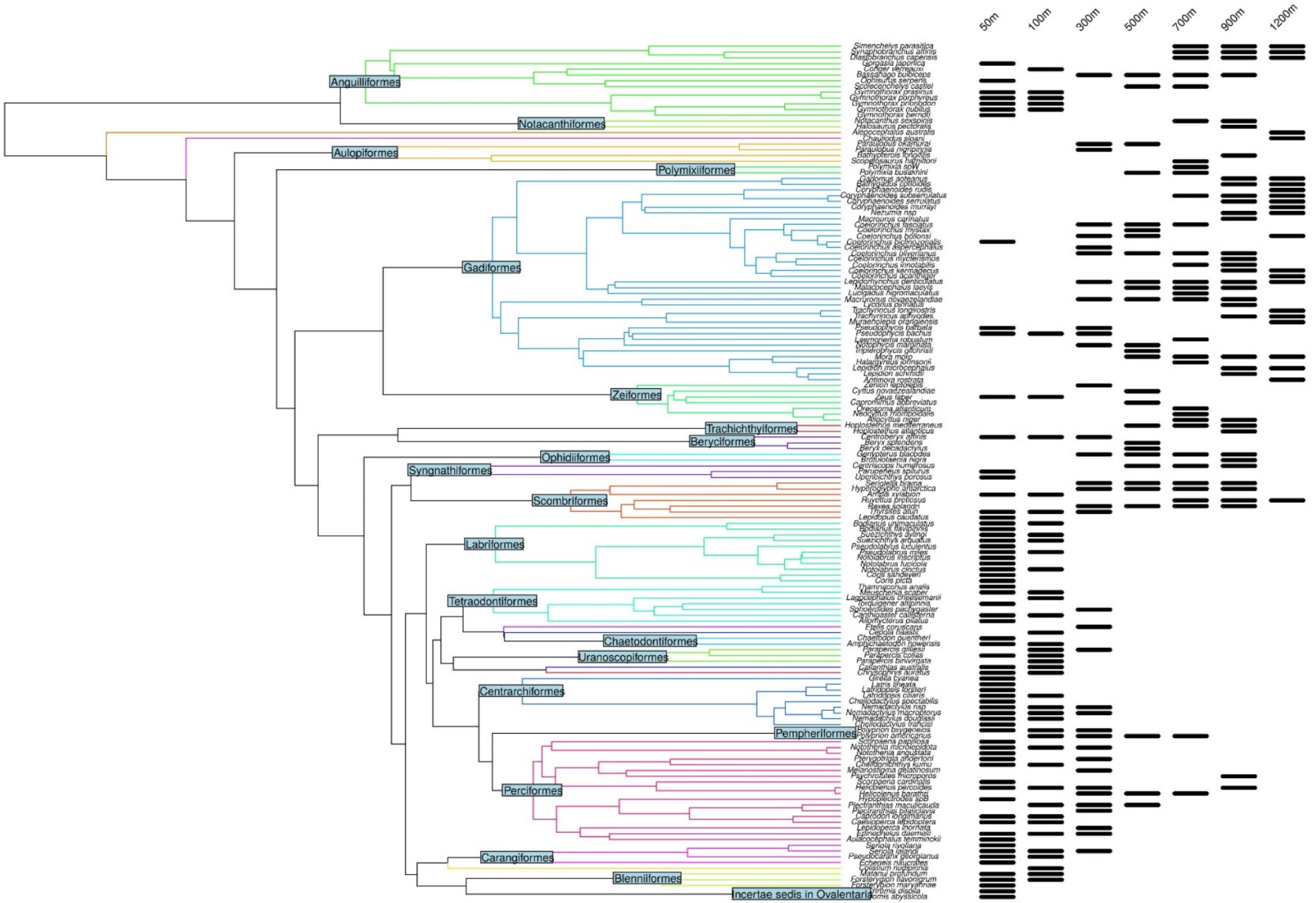

Figure A12: Maximum clade credibility tree (MCCT) including the 149 species present in the BRUV community dataset, with the species occurrence (in black) across depth but pooled across locations. Different colors correspond to different orders of fishes (class Actinopterygii).

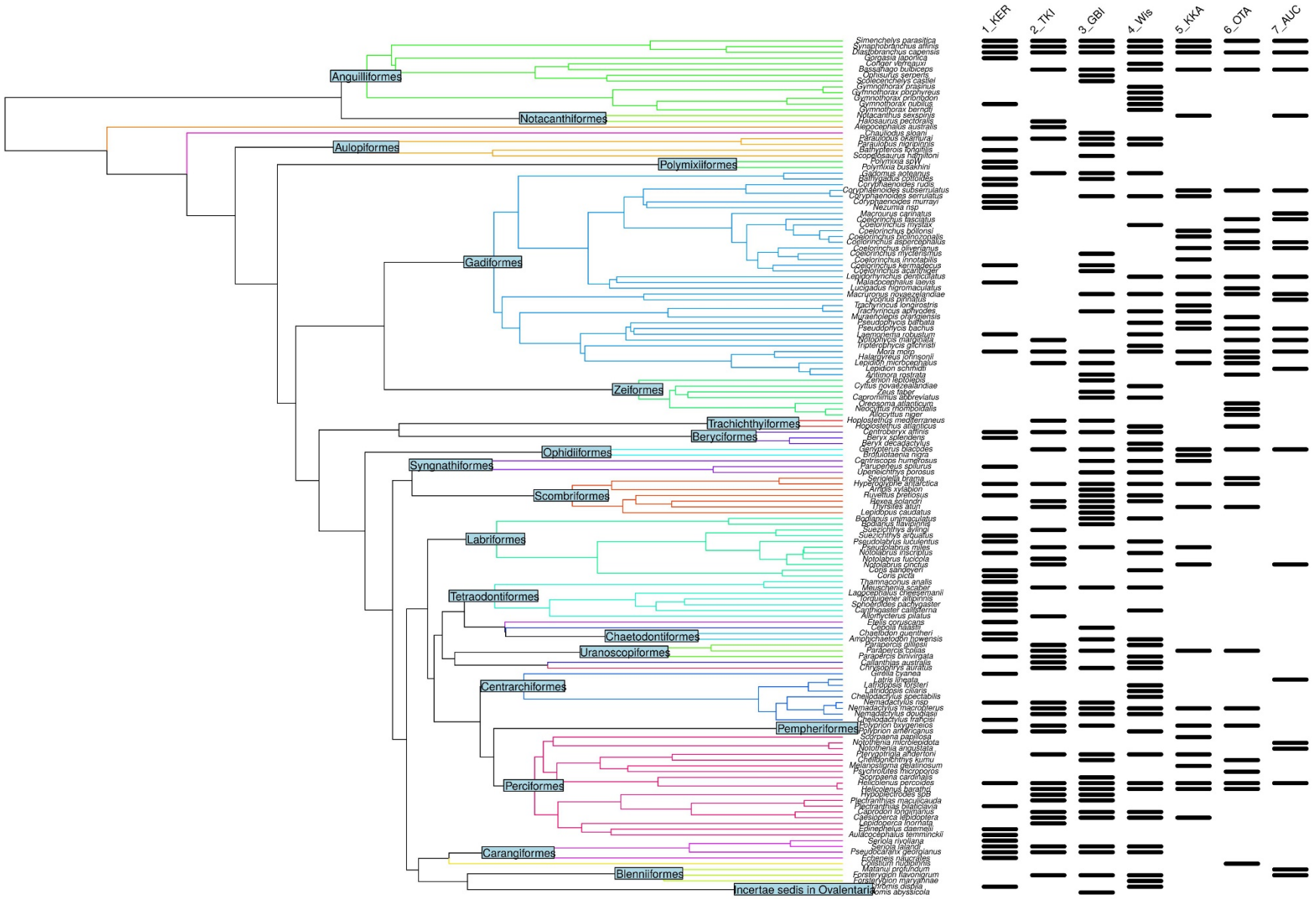

Figure A13: Maximum clade credibility tree (MCCT) including the 149 species present in the BRUV community dataset, with the species occurrence (in black) across latitude/locations but pooled across depth. Different colors correspond to different orders of fishes (class Actinopterygii). KER: Kermadec Islands, TKI: Three Kings Islands, GBI: Great Barrier Island, Wis: White Island, KKA: Kaikōura peninsula, OTA: Otago peninsula, AUC: Auckland Islands.

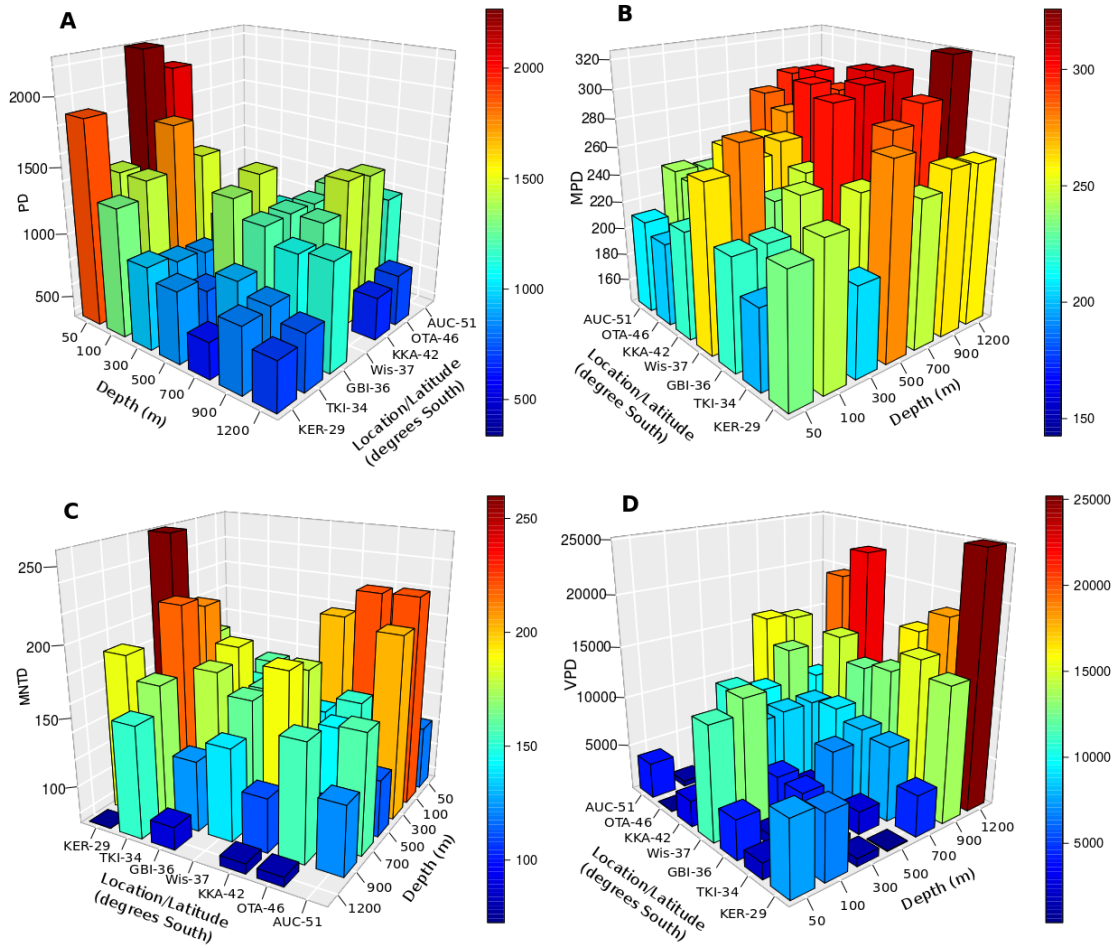

Figure A14: Three dimensional histograms showing the interaction between depth and latitude when considering the average value estimated over the 100 trees on the pooled 47 cell dataset, for phylogenetic diversity, PD (A), mean pairwise distance, MPD (B), mean nearest taxon distance, MNTD (C), and variance of the pairwise distance, VPD (D). The color gradient is related to each diversity measure separately, and the display of the depth and latitude axes may change from one panel to another to enable clear visualization of the interaction.

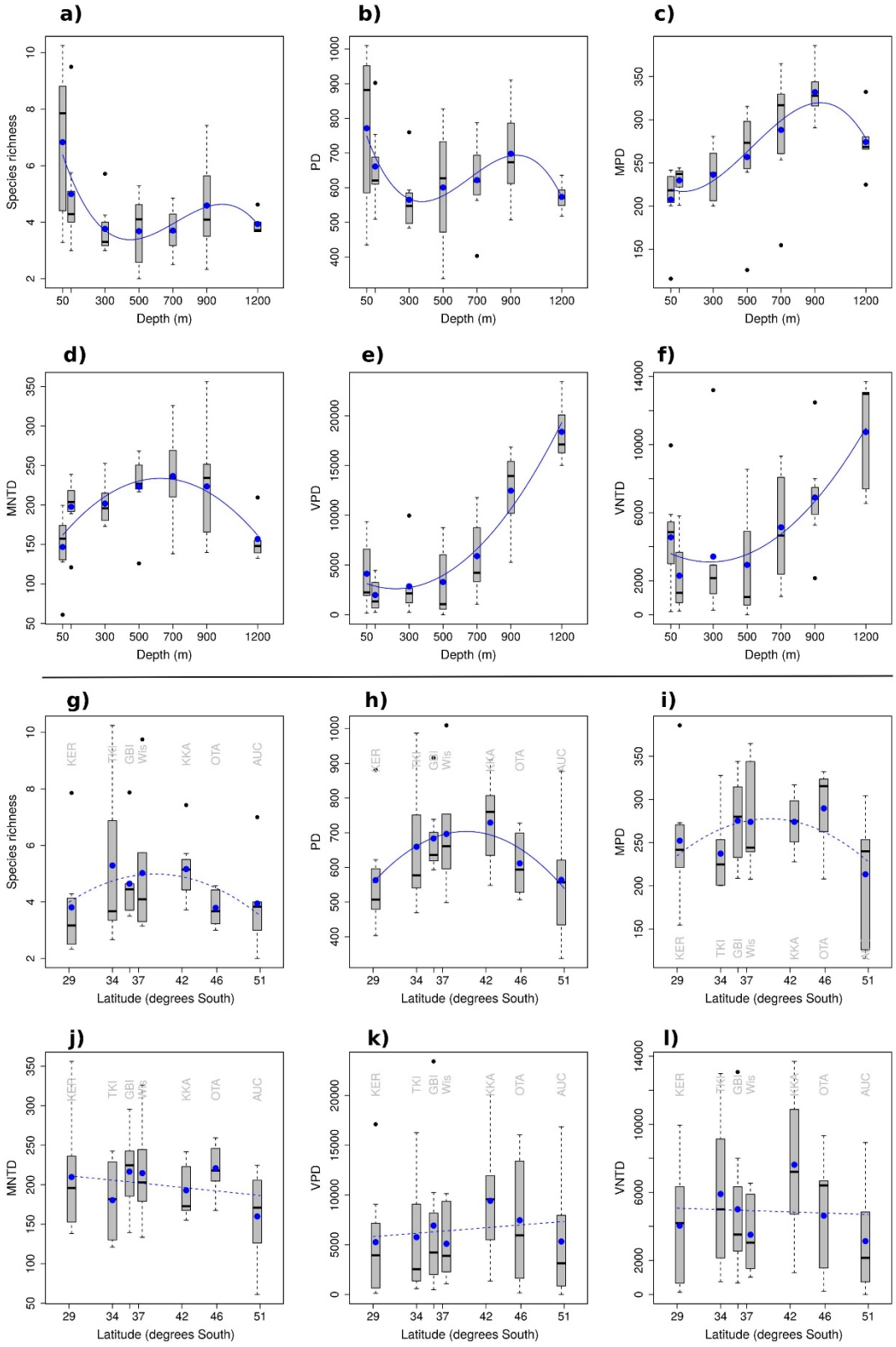

Figure A15: : Relationships of diversity indices with depth (top) and latitude (bottom), when considering the average value estimated over 100 trees on the average per BRUV 47 cells dataset for species richness (a, g), phylogenetic diversity, PD (b, h); mean pairwise distance, MPD (c, i); mean nearest taxon distance, MNTD (d, j); variance of the pairwise distance, VPD (e, k); and variance of the nearest taxon distance, VNTD (f, l). Black horizontal bars, black dots and boxes show the median,

outliers and interquartile range respectively. Whiskers are up to 1.5 times the interquartile range. Blue dots represent the average value per depth/latitude. For visualization purposes only, the blue curves represent the fit of the best model (dashed lines represent non-significant trends) selected based on AICc among three alternative models; model with a single term, a model with single and quadratic terms, and a model with single, quadratic and cubic terms for depth (a, b, c, d, e, f) or latitude (g, h, i, j, k, l). The model selection was performed separately for depth and latitude. The cubic term has been added in the model selection in order to improve the fit of the model for visualization purpose. For species richness, a generalized linear model with a negative binomial error model with a log link was used, for all other metrics we used an ordinary least square models with a Gaussian error, and identity link.

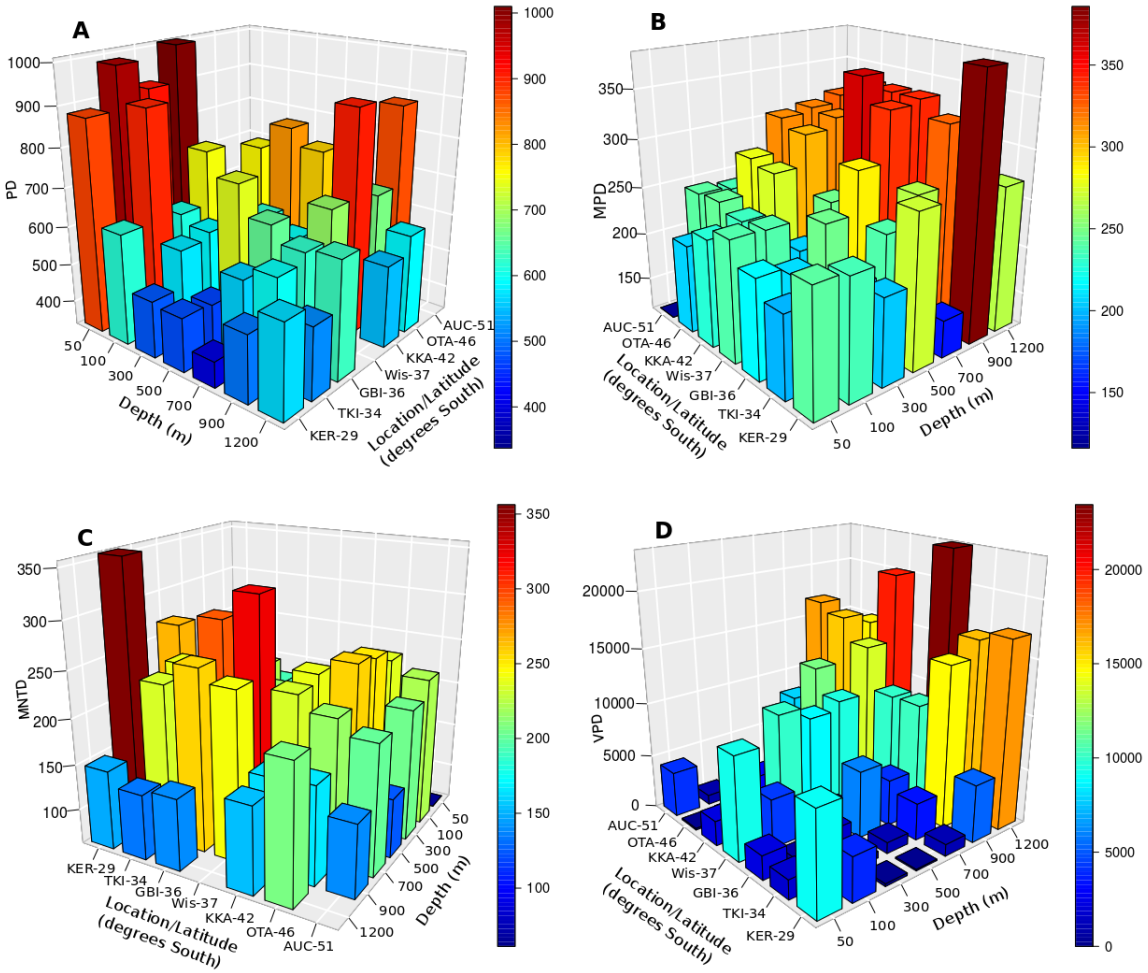

Figure A16: Three dimensional histograms showing the interaction between depth and latitude when considering the average value estimated over the 100 trees on the average per BRUV 47 cell dataset for: phylogenetic diversity, PD (A); mean pairwise distance, MPD (B); mean nearest taxon distance, MNTD (C); and variance of the pairwise distance, VPD (D). The color gradient is related to each diversity measure separately, and the display of the depth and latitude axes may change from one panel to another to enable clear visualization of the interaction.

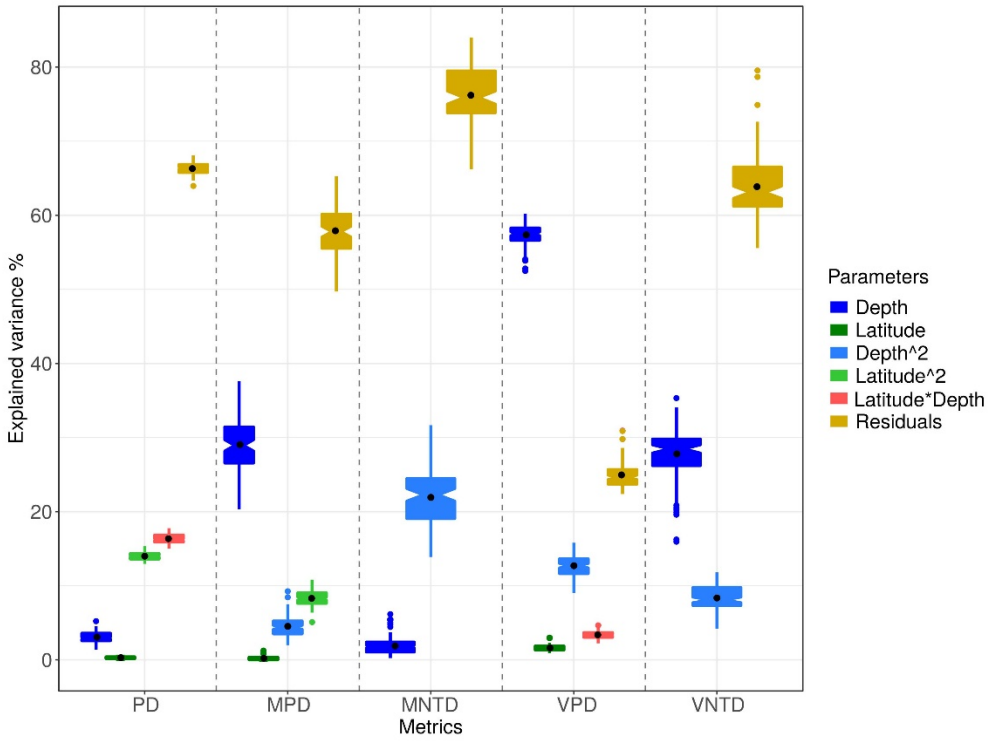

Figure A17: Variation in the proportion of explained variance for the different parameters retained in the best models for the 5 phylogenetic diversity metrics estimated over 100 trees, for the average per BRUV 47 cells dataset. Notch, black dots, color dots and boxes show the median, the average, the outliers and the interquartile range respectively. The maximum length of each whisker is 1.5 times the interquartile range. PD: phylogenetic diversity, MPD: mean pairwise distance, MNTD: mean nearest taxonomic distance, VPD: variance of the pairwise distance, VNTD: variance of the nearest taxonomic distance.

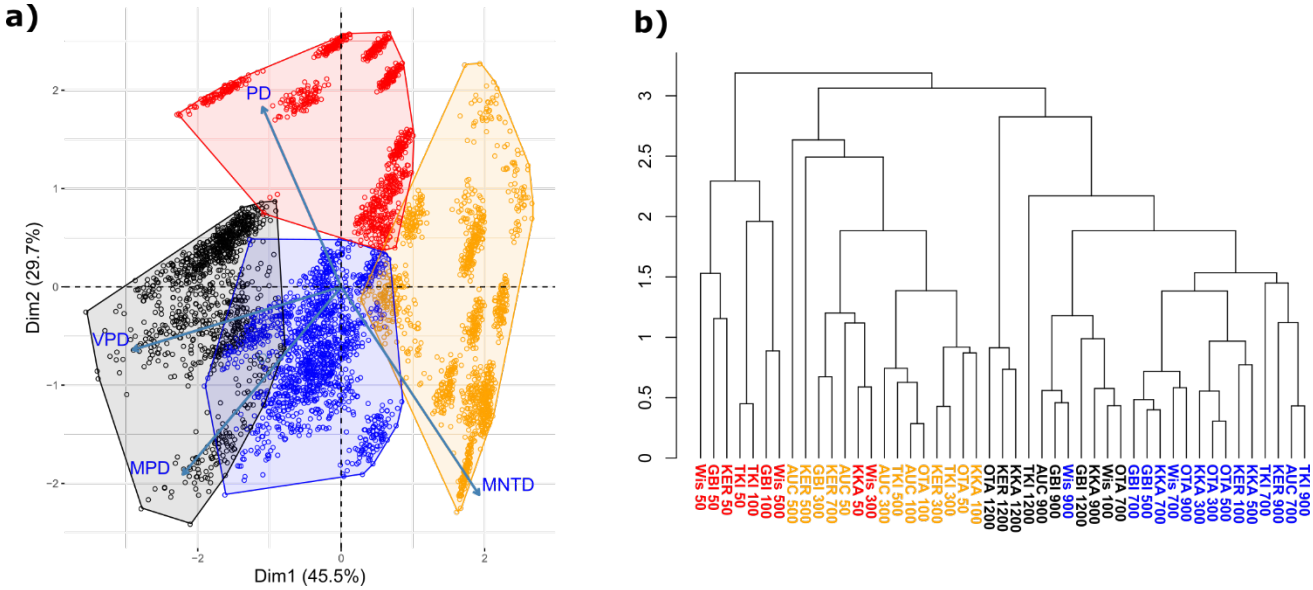

Figure A18: Phylogenetic bioregions across depth and latitude. **a)** Two dimensional PCA ordination plot showing the four clusters based on the 100 trees when using the pooled 47 cells dataset with phylogenetic diversity (PD), mean pairwise distance (MPD), variance of the pairwise distance (VPD), and mean nearest taxonomic distance (MNTD). The convex hull polygons show the envelope of the phylogenetic bioregions, showing the effect of the phylogenetic tree uncertainty on the clustering. **b)** Dendrogram built with an UPGMA algorithm using the 4 phylogenetic diversity measures extracted from the MCC tree allowing comparison with the hierarchical clustering based on the k-means approach. The color of the labels shows the four retained clusters based on the best grouping structure inferred by the k-means approach. The coefficient of correlation between the cophenetic distances of the UPGMA-derived dendrogram and the original distances is $r = 0.69$.

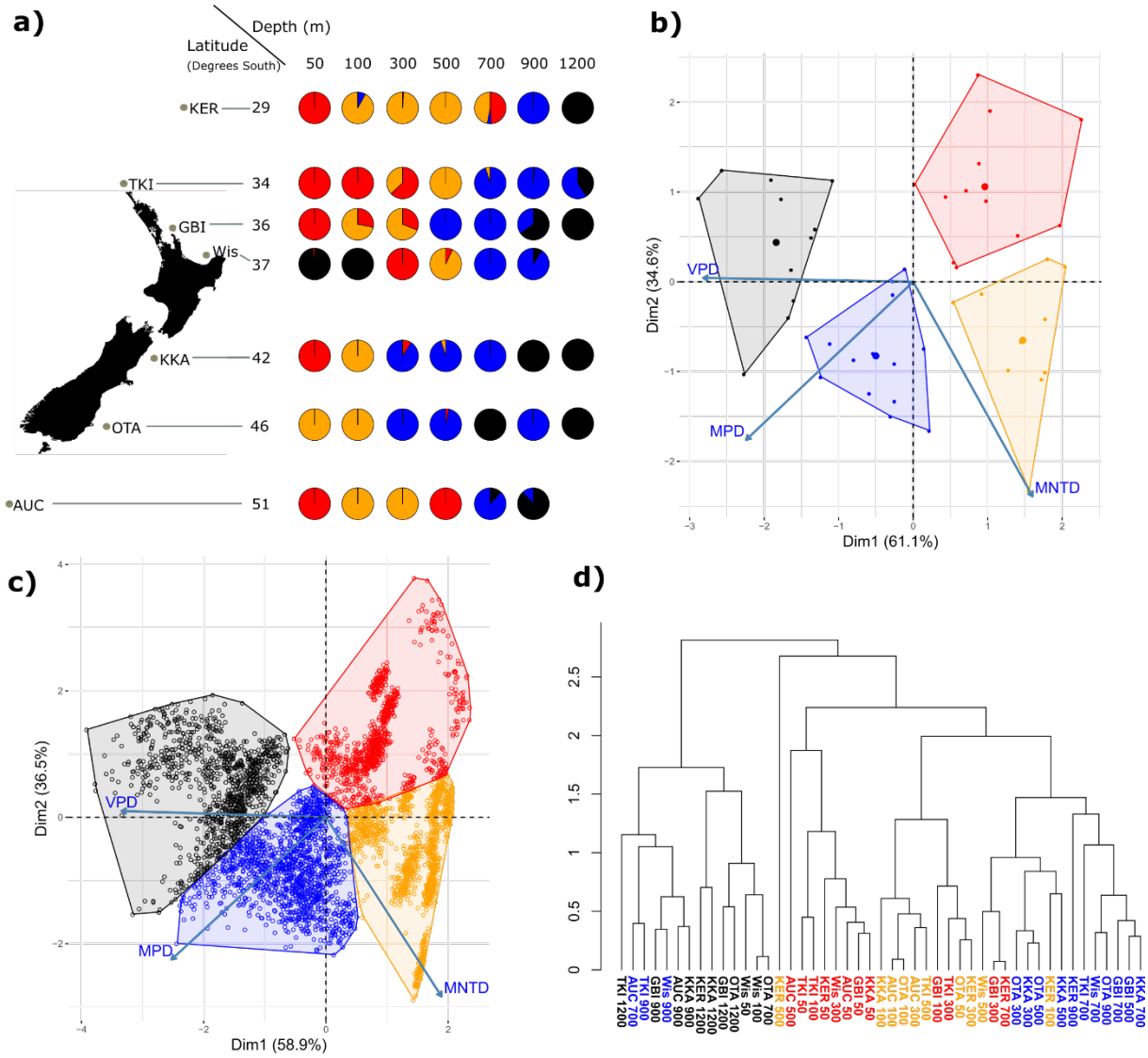

Figure A19: Phylogenetic bioregions across depth and latitude. **a**) The best groupings (k=4 clusters) across depth and latitude for the multivariate phylogenetic diversity measures including mean pairwise distance (MPD), variance of the pairwise distance (VPD), and mean nearest taxonomic distance (MNTD) based on the k-means approach realized over 100 trees for the pooled 47 cell dataset. Phylogenetic diversity (PD) was removed to decrease the strong influence of the species richness, and variance of the nearest taxonomic distance (VNTD) was also removed as it was not correlated with latitude or depth. The pies represent the proportion of trees supporting the samples in the four clusters. **b**) Two dimensional PCA ordination plot showing the four retained clusters using phylogenetic diversity measures extracted from the MCC tree with convex hull polygons showing the envelope of the phylogenetic bioregions. **c**) Two dimensional PCA ordination plot showing the four clusters based on 100 trees. **d)** Dendrogram built with a UPGMA algorithm using the 5 phylogenetic diversity measures extracted from the MCC tree allowing comparison with the hierarchical clustering based on the k-means approach. The color of the labels shows the four retained clusters based on the best grouping structure inferred by the k-means approach. The coefficient of correlation between the UPGMA-derived cophenetic distances of the dendrogram and the original distances is $r = 0.65$.

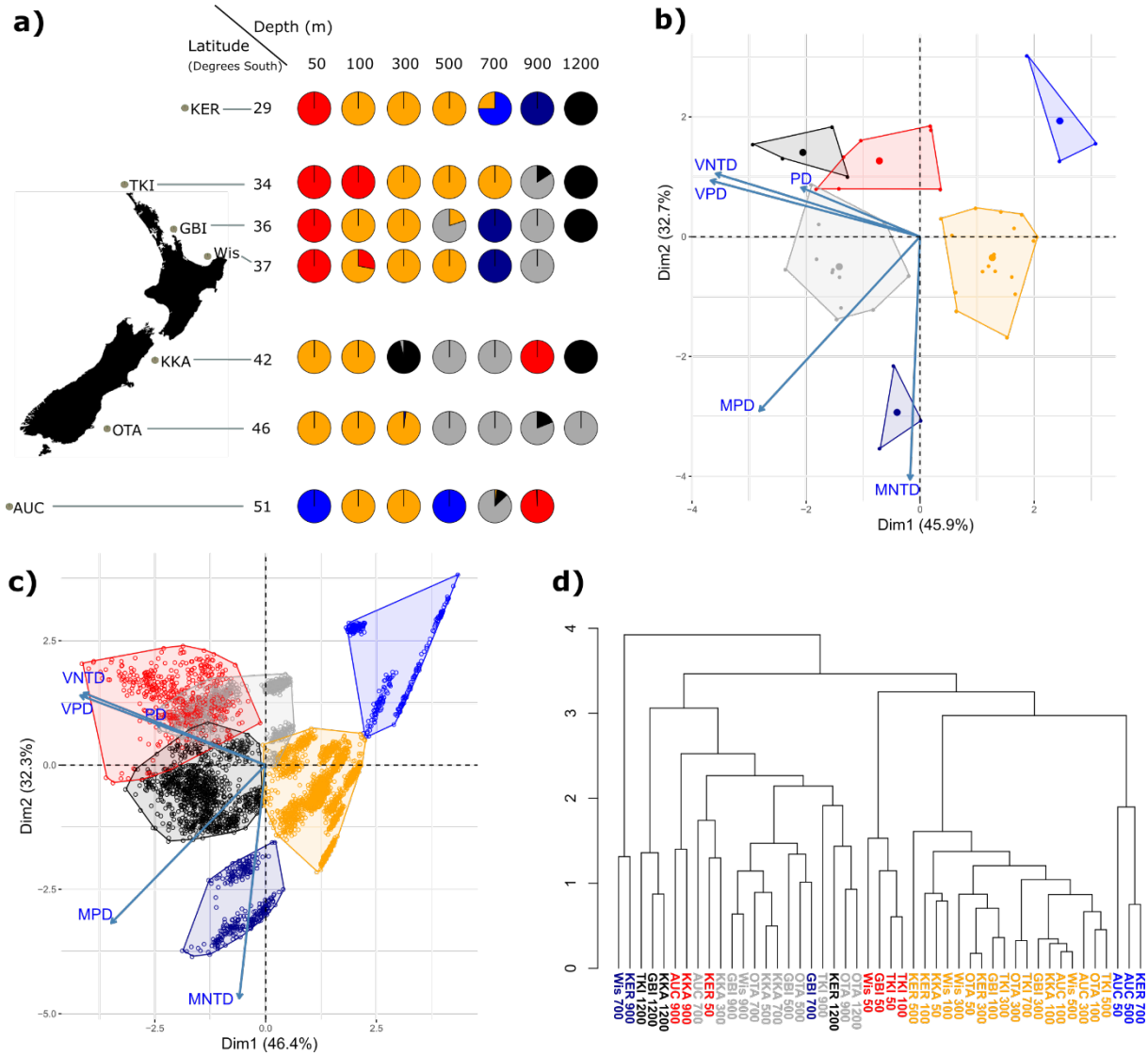

Figure A20: Phylogenetic bioregions across depth and latitude. **a**) The best groupings (k=6 clusters) across depth and latitude of the multivariate phylogenetic diversity measures including phylogenetic diversity (PD), mean pairwise distance (MPD), variance of the pairwise distance (VPD), mean nearest taxonomic distance (MNTD) and variance of the nearest taxonomic distance (VNTD) based on k-means approach realized over the 100 trees on the average per BRUV 47 cells dataset. The pies represent the proportion of trees supporting the samples in the six clusters. **b**) Two dimensional PCA ordination plot showing the six retained clusters using phylogenetic diversity measures extracted from the MCC tree; the convex hull polygons show the envelope of the phylogenetic bioregions. **c**) Two dimensional PCA ordination plot showing the four clusters based on 100 trees. **d)** Dendrogram built with a UPGMA algorithm using the 5 phylogenetic diversity measures extracted from the MCC tree allowing comparison with the hierarchical clustering based on the k-means approach. The color of the labels shows the six retained clusters based on the best grouping structure inferred by the k-means approach. The coefficient of correlation between the UPGMA-derived cophenetic distances of the dendrogram and the original distances is $r = 0.74$.

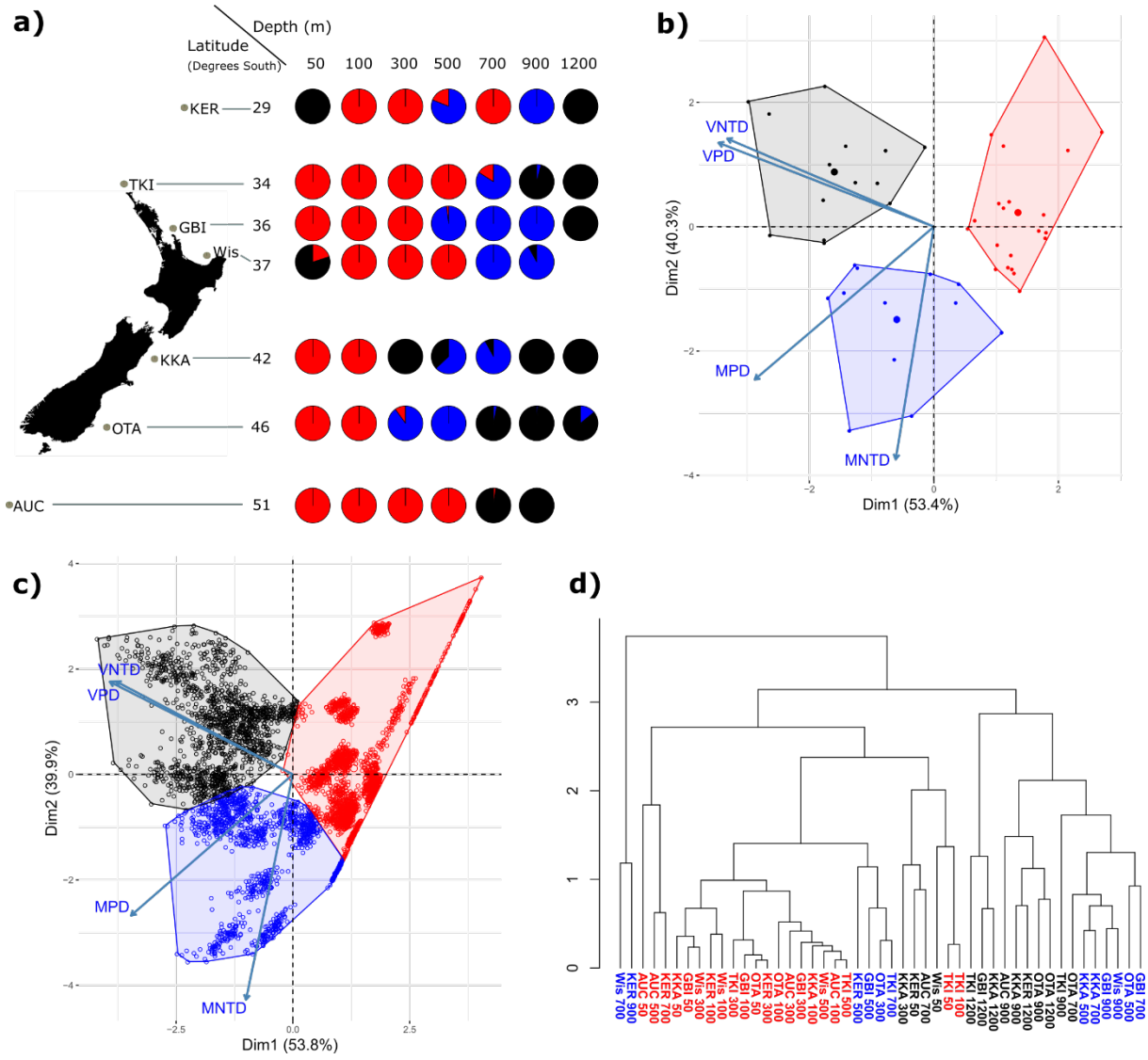

Figure A21: Phylogenetic bioregions across depth and latitude. **a**) The best groupings (k=3 clusters) across depth and latitude of the multivariate phylogenetic diversity measures including mean pairwise distance (MPD), variance of the pairwise distance (VPD), mean nearest taxonomic distance (MNTD) and variance of the nearest taxonomic distance (VNTD) based on k-means approach realized over the 100 trees on the average per BRUV 47 cells dataset. PD was removed to decrease the strong influence of the species richness. The pies represent the proportion of trees supporting the samples in the three clusters. **b**) Two dimensional PCA ordination plot showing the three retained clusters using phylogenetic diversity measures extracted from the MCC tree; the convex hull polygons show the envelope of the phylogenetic bioregions. **c**) Two dimensional PCA ordination plot showing the four clusters based on 100 trees. **d)** Dendrogram built with a UPGMA algorithm using the 4 phylogenetic diversity measures extracted from the MCC tree allowing comparison with the hierarchical clustering based on the k-means approach. The color of the labels shows the three retained clusters based on the best grouping structure inferred by the k-means approach. The coefficient of correlation between the UPGMA-based cophenetic distances of the dendrogram and the original distances is $r = 0.74$.

Table A2: Design of the four sets of candidate models considered in the model selection.

Design	Full model	Alternative models
ANOVA	Depth+Lat	1: Depth, 2: Lat
ANCOVA Latitude	Lat(factor)+Depth+Depth^2 +Lat*Depth+ Lat*Depth^2	1: Lat (factor)+Depth+Depth^2 +Lat*Depth, 2: Lat (factor)+Depth+Depth^2 , 3: Lat (factor)+Depth
ANCOVA Depth	Depth (factor)+Lat+Lat^2 +Depth*Lat+ Depth*Lat^2	1: Depth (factor)+Lat+Lat^2 +Depth*Lat, 2: Depth (factor)+Lat+Lat^2, 3: Depth (factor)+Lat
Linear with continuous variables	Depth+Lat+Depth^2 +Lat^2+Depth*Lat	1: Depth+Lat+Depth^2 +Lat^2, 2:Depth+Lat+Depth^2, 3:Depth+Lat+Depth^2+Depth*Lat, 4: Depth+Lat+Lat^2+Depth*Lat, 5:Depth+Lat +Lat^2, 6:Depth+Lat+Depth^2, 7:Depth+Lat+Depth*Lat, 8:Depth+ Lat, 9:Depth+depth^2, 10:Lat+Lat^2, 11: Depth, 12:Lat

Table A3: Parameter estimates, conditional and marginal R^2 and semipartial R^2 for the best linear mixed effect models considering a random intercept model for the tree (phylogenetic uncertainty) for the five phylogenetic diversity measures, considering the pooled 47 cells dataset. R^2.m. and R^2.c. represent the marginal R^2 and the conditional R^2 of Nakagawa and Shielzeth (2013) and Jonhson (2014), respectively. The former includes the fixed effects only, while the latter includes the fixed and the random effects. Semi.Partial marginal.R^2 and Semi.Partial Jaeger.R^2 represent the relative importance of specific fixed parameters in the model based on the Nakagawa, Shielzeth and Jonhson and Jaeger et al. (2017) approach, respectively. The Jaeger et al. (2017) approach considers the correlation effect among observations while it is ignored by the Nakagawa, Shielzeth and Jonhson approach. All the variables were normalized before the modeling to avoid numerical instability. The parameters with the higher semipartial R^2 are indicated in bold font.

Metrics	Random effect	Std.Rand	Std.Res	Parameter	Estimate	Std. Estimate	t-value	P.value	R^2.m.	R^2.c.	Semi.Partial. marginal.R^2	Semi.Partial. Jaeger.R^2
PD	Rand. Int.[1]	2.6*e-05	0.7	(Intercept)	0.272	0.019	14.34	0	0.51	0.51		
				Depth	-0.294	0.011	-26.56	0			**0.13**	**0.167**
				I(Depth^2)	0.112	0.012	9.78	0			0.02	0.026
				Latitude	-0.203	0.011	-19.23	0			0.073	0.095
				I(Latitude^2)	-0.361	0.011	-33.27	0			**0.19**	**0.239**
				Depth:Latitude	0.448	0.011	41.99	0			**0.273**	**0.333**
MPD	Rand. Int.	0.14	0.7	(Intercept)	0.442	0.024	18.88	0	0.49	0.51		
				Depth	0.692	0.011	62.64	0			**0.445**	**0.521**
				I(Depth^2)	-0.177	0.011	-15.55	0			**0.047**	**0.063**
				Latitude	0.019	0.011	1.88	0.061			0.001	0.001
				I(Latitude^2)	-0.265	0.011	-24.66	0			**0.111**	**0.144**
MNTD	Rand. Int.	2.2*e-08	0.78	(Intercept)	0.428	0.021	20.2	0	0.38	0.38		
				Depth	-0.018	0.012	-1.43	0.15			0	0.001
				Latitude	-0.117	0.012	-9.93	0			0.021	0.027
				I(Depth^2)	-0.568	0.013	-44.36	0			**0.295**	**0.358**
				I(Latitude^2)	0.123	0.012	10.19	0			0.022	0.029
				Depth:Latitude	-0.31	0.012	-26.06	0			**0.126**	**0.161**
VPD	Rand.Int	0.098	0.53	(Intercept)	-0.295	0.017	-17.47	1	0.69	0.7		
				Depth	0.655	0.011	60.41	0			**0.542**	**0.615**
				Latitude	0.071	0.008	8.75	0			0.015	0.02
				I(Depth^2)	0.337	0.009	36.76	0			**0.226**	**0.283**
				I(Latitude^2)	-0.038	0.008	-4.53	0			0.004	0.006
				Depth:Latitude	0.09	0.008	11.03	0			0.024	0.032
VNTD	Rand. Int.	3.4*e-05	0.98	(Intercept)	0.191	0.027	7.165	0	0.027	0.027		
				Depth	0.121	0.016	7.743	0			0.013	0.017
				Latitude	-0.004	0.015	-0.28	0.78			0	0
				I(Depth^2)	-0.091	0.016	-5.626	0			0.007	0.009
				I(Latitude^2)	-0.104	0.015	-6.823	0			0.01	0.013
				Depth:Latitude	-0.063	0.015	-4.179	0			0.004	0.005

[1]For Random intercept

Table A4: Parameter values and proportion of explained variance for the best models for the five phylogenetic diversity measures with depth and latitude, estimated across 100 trees extracted from the posterior distribution, for the average per BRUV 47 cells dataset. Significant P.values for the parameter estimates and the parameters that explained the most variance are indicated in bold font.

Metrics	Parameter	Estimate (sd)	Estimate range	Pvalue (sd)	Pvalue range	Explained variance % (sd)	Explained variance % range
PD	Intercept	-648.128 (44.277)	-747.568 – -550.691	0.382 (0.031)	0.31 – 0.446		
	Depth	-1.05 (0.033)	-1.144 – -0.957	**0.001 (0)**	0.001 – 0.002	3.072 (0.762)	1.383 – 5.216
	Latitude	78.639 (2.854)	72.532 – 85.576	**0.037 (0.005)**	0.026 – 0.047	0.298 (0.151)	0.02 – 0.677
	Latitude^2	-1.154 (0.039)	-1.253 – -1.067	**0.013 (0.002)**	0.009 – 0.018	**13.989 (0.518)**	12.944 – 15.347
	Depth*Latitude	0.025 (0.001)	0.023 – 0.028	**0.003 (0)**	0.002 – 0.004	**16.349 (0.563)**	15.002 – 17.769
MPD	Intercept	-405.493 (52.621)	-517.489 – -243.804	0.125 (0.033)	0.08 – 0.255		
	Depth	0.203 (0.016)	0.164 – 0.257	**0.006 (0.005)**	0 – 0.021	**29.045 (3.787)**	20.33 – 37.588
	Latitude	31.445 (2.838)	23.277 – 37.599	**0.021 (0.006)**	0.011 – 0.049	0.222 (0.25)	0 – 1.241
	Depth^2	0 (0)	0 – 0	0.08 (0.043)	0.008 – 0.212	4.528 (1.342)	1.978 – 9.252
	Latitude^2	-0.399 (0.037)	-0.479 – -0.296	**0.019 (0.005)**	0.01 – 0.044	**8.302 (1.045)**	5.089 – 10.828
MNTD	Intercept	147.656 (4.146)	137.041 – 156.595	**0 (0)**	0 – 0		
	Depth	0.263 (0.019)	0.218 – 0.326	**0.001 (0.001)**	0 – 0.006	1.883 (1.135)	0.235 – 6.164
	Depth^2	0 (0)	0 – 0	**0.002 (0.002)**	0 – 0.009	**21.925 (3.731)**	13.877 – 31.665
VPD	Intercept	7330.531 (933.191)	5410.113 – 9992.501	0.143 (0.022)	0.098 – 0.197		
	Depth	-26.852 (3.303)	-35.362 – -19.641	**0.007 (0.003)**	0.002 – 0.021	**57.352 (1.456)**	52.48 – 60.225
	Latitude	-94.61 (18.366)	-143.297 – -60.957	0.442 (0.051)	0.326 – 0.554	1.609 (0.359)	0.888 – 2.957
	Depth^2	0.019 (0.002)	0.012 –0.024	**0 (0)**	0 – 0	**12.706 (1.464)**	9.022 – 15.801
	Depth*Latitude	0.471 (0.072)	0.301 – 0.673	**0.024 (0.01)**	0.01 – 0.069	3.373 (0.462)	2.232 – 4.652
VNTD	Intercept	3874.385 (241.672)	3398.258 – 4433.314	**0.001 (0.001)**	0 – 0.006		
	Depth	-4.798 (1.034)	-7.37 – -2.48	0.307 (0.114)	0.115 – 0.612	**27.799 (3.559)**	15.945 – 35.321
	Depth^2	0.009 (0.001)	0.005 – 0.013	**0.027 (0.022)**	0.004 – 0.133	8.351 (1.725)	4.227 – 11.805

Table A5: Parameter estimates, conditional and marginal R^2 and semipartial R^2 for the best linear mixed effect models considering a random intercept model for the tree (Phylogenetic uncertainty) for the five phylogenetic diversity measures, considering the average per BRUV 47 cells dataset. R^2.m. and R^2.c. represent the marginal R^2 and the conditional R^2 of Nakagawa and Shielzeth (2013) and Jonhson (2014), respectively. The former includes the fixed effects only while the latter includes the fixed and the random effects. Semi.Partial marginal.R^2 and Semi.Partial Jaeger.R^2 represent the relative importance of specific fixed parameters in the model based on the Nakagawa, Shielzeth and Jonhson and Jaeger et al. (2017) approach, respectively. The Jaeger et al. (2017) approach takes into account the correlation effect among observations while it is ignored by the Nakagawa, Shielzeth and Jonhson approach. All the variables were normalized before the modeling to avoid numerical instability. Parameters with the highest semipartial R^2 are indicated in bold font.

Metrics	Random effect	Std.Rand	Std.Res	Parameter	Estimate	Std. Estimate	t-value	P.value	R^2.m.	R^2.c.	Partial. marginal.R^2	Partial. Jaeger.R^2
PD	Rand. Int.[1]	6.3*e-08	0.799	(Intercept)	0.16315	0.0216	7.55	0	0.363	0.363		
				Depth	-0.22378	0.0126	-17.76	0			0.063	0.082
				I(Depth^2)	0.19573	0.01306	14.99	0			0.046	0.06
				Latitude	0.05235	0.01202	4.36	0			0.004	0.005
				I(Latitude^2)	-0.33533	0.01232	-27.21	0			**0.136**	**0.173**
				Depth:Latitude	0.43657	0.01214	35.97	0			**0.216**	**0.268**
MPD	Rand. Int.	0.036	0.766	(Intercept)	0.52783	0.02099	25.14	0	0.412	0.414		
				Depth	0.61371	0.01209	50.78	0			**0.354**	**0.422**
				I(Depth^2)	-0.23212	0.01252	-18.54	0			0.068	0.089
				Latitude	0.02354	0.01152	2.04	0.0413			**0.115**	**0.148**
				I(Latitude^2)	-0.29265	0.01182	-24.76	0			0.001	0.001
				Depth:Latitude	0.05876	0.01164	5.05	0			0.005	0.007
MNTD	Rand. Int.	0.00E+00	0.82	(Intercept)	0.74811	0.02218	33.72	0	0.328	0.328		
				Depth	0.30685	0.01294	23.71	0			**0.107**	**0.137**
				Latitude	-0.15297	0.01234	-12.4	0			0.032	0.042
				I(Depth^2)	-0.55334	0.01341	-41.27	0			**0.266**	**0.325**
				I(Latitude^2)	-0.20457	0.01266	-16.16	0			0.053	0.069
				Depth:Latitude	-0.17863	0.01246	-14.33	0			0.042	0.055
VPD	Rand.Int	0.084	0.507	(Intercept)	-0.320124	0.016052	-19.94	0	0.736	0.743		
				Depth	0.615564	0.008001	76.94	0			**0.55**	**0.622**
				Latitude	0.170508	0.007629	22.35	0			0.094	0.122
				I(Depth^2)	0.409085	0.00829	49.35	0			**0.335**	**0.404**
				I(Latitude^2)	-0.079256	0.007825	-10.13	0			0.021	0.028
				Depth:Latitude	0.178389	0.007706	23.15	0			0.1	0.13
VNTD	Rand. Int.	5.1*e-09	0.78	(Intercept)	-0.14692	0.02111	-6.96	0	0.391	0.391		
				Depth	0.4072	0.01231	33.07	0			**0.189**	**0.236**
				Latitude	0.06921	0.01174	5.89	0			0.007	0.01
				I(Depth^2)	0.32304	0.01276	25.32	0			**0.12**	**0.154**

				I(Latitude^2)	-0.17144	0.01204	-14.24	0			0.041	0.054
				Depth:Latitude	0.08603	0.01186	7.25	0			0.011	0.015

[1]For Random intercept

REFERENCES

Alfaro, M.E. et al. 2018. Explosive diversification of marine fishes at the Cretaceous-Palaeogene boundary. - Nat. Ecol. Evol. 2: 688–696.

Alroy, J. 2008. Dynamics of origination and extinction in the marine fossil record. - Proc. Natl. Acad. Sci. 105: 11536–11542.

Alroy, J. 2010. The shifting balance of diversity among major marine animal groups. - Science 329: 1191–1194.

Bartoń, K. 2016. MuMIn: Multi-Model Inference. R package version 1.15.6. available at: https://CRAN.R-project.org/package=MuMIn.

Bates, D. et al. 2015. Fitting Linear Mixed-Effects Models Using lme4. - J. Stat. Softw. 67: 1–48.

Betancur-R, R. et al. 2013a. The Tree of Life and a New Classification of Bony Fishes. - PLOS Curr. Tree Life 0732988: 1–45.

Betancur-R, R. et al. 2013b. Addressing gene tree discordance and non-stationarity to resolve a multi-locus phylogeny of the flatfishes (Teleostei: Pleuronectiformes). - Syst. Biol. 62: 763–785.

Betancur-R, R. et al. 2015. Fossil-based comparative analyses reveal ancient marine ancestry erased by extinction in ray-finned fishes. - Ecol. Lett. 18: 441–450.

Betancur-R, R. et al. 2017. Phylogenetic classification of bony fishes. - BMC Evol. Biol. 17: 162.

Bouckaert, R. et al. 201. BEAST 2: A Software Platform for Bayesian Evolutionary Analysis. - PLOS Comput. Biol. 10: 1–6.

Capella-Gutíerrez, S. et al. 2009. TrimAl: a tool for automatic alignment trimming. - Bioinformatics 25: 1972–1973.

Castresana, J. 2000. Selection of conserved blocks from multiple alignments for their use in phylogenetic analysis. - Mol. Biol. Evol. 17: 540–552.

Cusimano, N. et al. 2012. A new method for handling missing species in diversification analysis applicable to randomly or nonrandomly sampled phylogenies. - Syst. Biol. 61: 785–792.

Davis, M. P. et al. 2013. Exploring power and parameter estimation of the BiSSE method for analyzing species diversification. - BMC Evol. Biol. 13: 13–38.

Drummond, A.J. et al. 2006. Relaxed phylogenetics and dating with confidence. - PLOS Biol. 4: 699–710.

Eme, D. et al. 2019. An integrated pathway for building regional phylogenies for ecological studies. Glob. Ecol. Biogeogr. 28: 1899-1911.

Eme, D. et al. 2020. Data from: Phylogenetic measures reveal eco-evolutionary drivers of biodiversity along a depth gradient, Dryad, Dataset, https://doi.org/10.5061/dryad.0rxwdbrw1

Fitzjohn, R.G. et al. 2009. Estimating trait-dependent speciation and extinction rates from incompletely resolved phylogenies. - Syst. Biol. 58: 595–611.

Fitzjohn, R. G. 2012. Diversitree: Comparative phylogenetic analyses of diversification in R. - Methods Ecol. Evol. 3: 1084–1092.

Harnik, P.G. et al. 2012. Extinctions in ancient and modern seas. - Trends Ecol. Evol. 27: 608–617.

Henao Diaz, L.F. et al. 2019. Macroevolutionary diversification rates show time dependency. - Proc. Natl. Acad. Sci. U. S. A. 116: 7403-7408.

Hewitt, G.M. 2004. Genetic consequences of climatic oscillations in the Quaternary. - Phil. Trans. R. Soc. B. 359: 183-195.

Höhna, S. 2010. Likelihood Inference of Non-Constant Diversification Rates with Incomplete Taxon Sampling. - PlOS one, 5: 1–8.

Höhna, S. 2013. Fast simulation of reconstructed phylogenies under global time-dependent birth-death processes. - Bioinformatics 29: 1367–1374.

Höhna, S. et al. 2011. Inferring speciation and extinction rates under different sampling schemes. - Mol. Biol. Evol. 28: 2577–2589.

Hughes L.C. et al. 2018. Comprehensive phylogeny of ray-finned fishes (Actinopterygii) based on transcriptomic and genomic data. - Proc. Natl. Acad. Sci. U. S. A. 115: 6249-6254.

Ivanova, N. V. et al. 2007. Universal primer cocktails for fish DNA barcoding. - Mol. Ecol. Notes **7**: 544-548.

Jablonski, D. 2008. Extinction and the spatial dynamics of biodiversity. - Proc. Natl. Acad. Sci. U. S. A. 105: 11528–11535.

Jaeger, B. 2017. r2glmm: Computes R Squared for Mixed (Multilevel) Models. R package version 0.1.2. Available at: https://CRAN.R-project.org/package=r2glmm.

Jaeger, B.C. et al. 2017. An R statistic for fixed effects in the generalized linear mixed model. - J. Appl. Stat. 44: 1086–1105.

Jetz, W. and Pyron, R.A. 2018. The interplay of past diversification and evolutionary isolation with present imperilment across the amphibian tree of life. - Nat. Ecol. Evol. 2: 850–858.

Jetz, W. et al. 2012. The global diversity of birds in space and time. - Nature 491: 444–8.

Johnson, P.C.D. 2014. Extension of Nakagawa and Schielzeth's R 2GLMM to random slopes models. - Methods Ecol. Evol. 5: 944–946.

Kocsis, Á.T. et al. 2019. The r package divDyn for quantifying diversity dynamics using fossil sampling data. - Methods Ecol. Evol. 10: 735–743.

Krug, A.Z. et al. 2009. Signature of the end-cretaceous mass extinction in the modern biota. - Science 323: 767–771.

Kuhn, T.S. et al. 2011. A simple polytomy resolver for dated phylogenies. - Methods Ecol. Evol. 2: 427–436.

Lanfear R. et al. 2017. PartitionFinder 2: New Methods for Selecting Partitioned Models of Evolution for Molecular and Morphological Phylogenetic Analyses. - Mol. Biol. and Evol. 34: 772–773.

López, J. A. et al. 2004. Esociform phylogeny. - Copeia, 2004: 449-464.

Matschiner M. et al. 2017. Bayesian phylogenetic estimation of clade ages supports trans-Atlantic dispersal of cichlid fishes. - Syst. Biol. 66: 3–22.

Morlon, H. 2014. Phylogenetic approaches for studying diversification. – Ecol. Lett. 17: 508–525.

Morlon, H. et al. 2011. Reconciling molecular phylogenies with the fossil record. - Proc. Natl. Acad. Sci. U. S. A. 108: 16327–16332.

Nakagawa, S. and Schielzeth, H. 2013. A general and simple method for obtaining R 2 from generalized linear mixed-effects models. - Methods Ecol. Evol. 2: 133–142.

Near T.J. et al. 2013. Phylogeny and tempo of diversification in the superradiation of spiny-rayed fishes. - Proc. Natl. Acad. Sci. U. S. A. 110: 12738–12743.

Near T.J., et al. 2012. Resolution of ray-finned fish phylogeny and timing of diversification. - Proc. Natl. Acad. Sci. U. S. A. 109: 13698–13703.

Paradis, E. and Schliep, K. 2019. Ape 5.0: An environment for modern phylogenetics and evolutionary analyses in R. - Bioinformatics 35: 526–528.

Pinheiro, J. et al. 2016. nlme: Linear and Nonlinear Mixed Effects Models. R package version 3.1-128, available at: http://CRAN.R-project.org/package=nlme.

R Development Core Team, (2018) R: a language and environment for statistical computing. R Foundation for Statistical Computing, Vienna. Available at: http://www.R-project.org.

Rabosky, D.L. 2010. Extinction rates should not be estimated from molecular phylogenies. - Evolution 64: 1816–1824.

Rabosky, D.L. et al. 2018. An inverse latitudinal gradient in speciation rate for marine fishes. - Nature 559: 392–395.

Rabosky, D.L. et al. 2013. Rates of speciation and morphological evolution are correlated across the largest vertebrate radiation. - Nature Com. **4**, 1–8.

Rambaut A. et al. 2013. Tracer V1.6. Available at: http://tree.bio.ed.ac.uk/software/tracer/

Roberts, C.D. et al. 2017. Checklist of the Fishes of New Zealand: Online Version 1.0. Museum of New Zealand Te Papa Tongarewa, Wellington Version 1.0: pages 1–176, first published on Te Papa website, 7 July 2017. Available at: https://www.tepapa.govt.nz/sites/default/files/checklist_of_the_fishes_of_new_zealand_v_1_0_july_2017.pdf

Sanmartín, I. and Meseguer, A.S. 2016. Extinction in phylogenetics and biogeography: From timetrees to patterns of biotic assemblage. - Front. Genet. **7**: 1–17.

Santini F. et al. 2009. Did genome duplication drive the origin of teleosts? A comparative study of diversification in ray-finned fishes. - BMC Evol. Biol. 9, 1–15.

Stadler, T. 2011. Mammalian phylogeny reveals recent diversification rate shifts. - Proc. Natl. Acad. Sci. U. S. A. 108: 6187–6192.

Stamatakis A. 2014. RAxML version 8: A tool for phylogenetic analysis and post-analysis of large phylogenies. - Bioinformatics 30: 1312–1313.

Venables, W.N. and Ripley, B. D. 2002. Modern Statistics with S. fourth Edition. Springer, New York.

Walsh P. et al. 1991. Chelex 100 as a medium for simple extraction of DNA for PCR-based typing from forensic material. - Biotechniques 10: 506-513.

Ward, R. D. et al. 2005. DNA barcoding Australia's fish species. Phil. Trans. R. Soc. B. 360: 1847-1857.

Zuur, A. et al. 2010. Mixed effects models and extension in ecology with R. – Springer.